Monitoring Soil Moisture and Freeze/Thaw State Using C-band Imaging Radar

by

Wen Tang

A thesis
presented to the University of Waterloo
in fulfillment of the
thesis requirement for the degree of
Master of Science
in
Geography

Waterloo, Ontario, Canada, 2015

© Wen Tang 2015

Author's Declaration

I hereby declare that I am the sole author of this thesis. This is a true copy of the thesis, including any required final revisions, as accepted by my examiners.

I understand that my thesis may be made electronically available to the public.

Abstract

Soil moisture is an important state variable in many hydrological and meteorological applications. This thesis explores the use of the C-band synthetic aperture radar (SAR) parameters to monitor soil moisture and freeze/thaw state in a cold-season hydrologic environment. The circular-linear compact polarimetric (CP) configuration is considered as a possible alternative of the quad polarimetric (QP) system because it acquires images with wider swath and reduced complexity, cost and energy requirement of the radar system while maintaining the information content of the acquired imagery. In this study, 15 RADARSAT-2 QP images were acquired from October 2013 to June 2014 and CP images were simulated from each RADARSAT-2 QP imagery acquired. Field measurements of soil properties were collected along with the radar imagery acquisitions. The backscattering coefficients in all polarizations were able to discriminate frozen and unfrozen soils. But their correlations with soil moisture content were weak if examining frozen or unfrozen soils separately. The Oh et al. (1992) model was implemented in this study to compare with acquired RADARSAT-2 data. A good agreement was found between the linear polarimetric backscattering coefficients simulated by the Oh model and the RADARSAT-2 data, indicating that the study site even with 10 cm tall standing hay was consistent with a bare soil site at C-band and the Oh model can be applied to frozen soils. With respect to CP parameters, the first and fourth Stokes parameters and $m - \delta$ surface and volume scattering components can detect soil freeze/thaw state and have potential for frozen/unfrozen soils mapping. The influence of vegetation on selected CP parameters was also evident in this study. Results demonstrated the utility of C-band radar in detecting soil freeze/thaw state rather than monitoring the changes of soil moisture content. More image acquisitions during the freezing and thawing periods, continuous field measurements of soil moisture and state, and

ground measurements collected over wider study area can help further develop understanding of the CP parameters and facilitate future use of the CP mode. The contribution of this thesis is to provide better understanding of the CP parameters at a specific site and to demonstrate that CP parameters can replicate QP SAR variables to detect surface soil conditions.

Acknowledgements

To my dear brothers and sisters in MCCF and church, thanks everyone for always walking with me and praying for me, especially during my hard times. I am very thankful to know everyone. I hope that we will continue the walk together in Jesus Christ.

Table of Contents

List of Tables

List of Figures

Chapter 1

Introduction

1.1 Introduction

Soil moisture is defined generally as the amount of water contained in the unsaturated soil zone (Hillel, 1998). It is a key state variable of the global energy and water cycles and influences the exchange of energy and water at the surface/atmosphere interface. Soil moisture has impacts on climate processes, such as air temperature and precipitation, through its effect on the partitioning of the incoming energy in the latent and sensible heat fluxes (Brubaker et al, 1993; Durre et al, 2000). It is a major source of water for the atmosphere through the process of evapotranspiration. Over land surfaces, approximately two thirds of the total precipitation is evapotranspired by the plants and soil (Shukla and Mintz, 1982). Soil moisture is also linked to biogeochemical cycles, such as carbon and nitrogen cycles, through the processes of plant transpiration and photosynthesis (Seneviratne et al., 2010). Hydrologically, antecedent soil moisture state is an important variable controlling processes of infiltration and surface runoff. It influences the soil's capacity to respond to rainfall or snowmelt events by determining whether infiltration or runoff occurs (Dingman, 2002). Overland flow will occur on saturated soils and cause soil erosion (Dingman, 2002). Thus, knowledge of the spatial distribution of soil moisture helps to determine the potential for infiltration, overland flow, floods, erosion and impacts on streams, reservoirs and infrastructure.

Frozen soil can affect the decomposition of organic substances and the biota living in the soil (Niu and Yang, 2006). It also reduces the soil permeability and impedes water infiltration. If the soil with high water content freezes, a concrete impermeable frost forms and prevents infiltration, thus creating increased potential for soil erosion during spring thaw and/or rainfall events (Hillard et al, 2003). In addition, the runoff can transport contaminants from agricultural sources to streams, which adversely affect the surface water quality (Ulén, 2003). Therefore, freeze/thaw state of soils is an important attribute for agricultural production and environmental sustainability.

Given the important roles which the soil moisture and its freeze/thaw state play in climate and water resource management, extensive studies have been conducted to provide knowledge and measurements of soil conditions at global, regional and local scales. *In situ* soil moisture measurements are labour intensive and costly, and therefore impractical to be carried out over areas larger than a few watersheds (Kornelsen and Coulibaly, 2013). Remote sensing offers an alternative for improved characterization of the distribution and amount of water in soils at various scales. Active microwave remote sensing is particularly applicable owing to its sensitivity to the dielectric properties of soil, which are dependent on water and ice content (Hallikainen et al. 1985; Schmugge, 1985; Dobson and Ulaby, 1986). Microwave imaging sensors, such as synthetic aperture radar (SAR), use their own source of illumination which enables all-weather monitoring of the Earth surface at high spatial resolution (i.e. meters to tens of meters) (Richards, 2009; Ulaby et al., 1981). Experimental results and studies have demonstrated that low frequency microwaves, such as C-band, can successfully detect changes of surface soil moisture conditions (Ulaby et al., 1978; Dobson and Ulaby, 1986; Geng et al, 1996; Baghdadi et al., 2006). In addition, the C-band SAR signals can penetrate dry snow

(Bernier and Fortin, 1998; Pivot, 2012) thus providing an opportunity to observe the underlying soil conditions during the winter.

The sensitivity of linear polarizations (HH, HV, VH and VV) to soil moisture has been extensively studied in recent years with the availability of full polarimetric data. The full or quad polarimetric (FP or QP) SAR sensor transmits and receives both horizontally and vertically polarizations. It is expected to provide the most information about the target feature since it records the complete characterization of the scattering behavior from a target (Charbonneau et al., 2010). However, the QP system suffers from narrow swath coverage, increased complexity of the radar system, and high power requirement for the transmitter (Charbonneau et al., 2010). As a result, the dual polarimetric (DP) system is widely investigated as a possible alternative of the QP system. The DP system transmits one polarization and receives two (eg. HH and HV, or VH and VV). Research in the DP system has led to the compact polarimetry (CP), which overcomes many engineering disadvantages of the QP system while maintaining the information content of images. Three CP operation modes have been introduced in literature: 1) $\pi/4$ mode, which transmits a linear polarization oriented at 45° with respect to the horizontal or vertical polarization and receives both horizontal and vertical polarizations (Souyris et al., 2005); 2) dual circular polarimetric mode, which transmits right (or left) circular polarization and receives both right and left circular polarizations (Stacy and Preiss, 2006); 3) circular-linear polarimetric (CL-pol) mode, also refers to hybrid polarity, which transmits right circular polarization and receives both horizontal and vertical components (Raney, 2007). The CL-pol mode has been added to the system design of the Canadian RADARSAT Constellation Mission (RCM), which is planned to be launched in 2018 (Canadian Space Agency, 2013). However, very few studies on soil

moisture and freeze/thaw state using the CP data have been conducted. Therefore, more research is needed to further investigate the new CP mode and support the future satellite mission.

1.2 Goal and Objectives

The main goal of this research is to assess the utility of the circular-linear CP mode in a soil moisture and freeze/thaw application of a cold-season hydrologic environment by comparing the information content of the CP data with the RADARSAT-2 QP observations and Oh model estimates. The following three specific objectives are defined:

1) A review of the current knowledge of QP and CP radar systems and SAR parameters for soil moisture and freeze/thaw applications;

2) An analysis of the ground measurements, RADARSAT-2 QP backscatter and Oh model estimates to characterize the physical nature of the study site;

3) A sensitivity analysis of CP parameters to soil moisture and freeze/thaw state with the established knowledge from (1) and (2).

1.3 Thesis Structure

The remainder of this thesis is organized into the following chapters. Chapter 2 provides a background review of the radar polarimetry and active remote sensing of soil. It includes a detailed description of different radar systems and the current state of knowledge of radar remote sensing of soil. Chapter 3 consists of a paper entitled "The potential of using RADARSAT-2 quad polarimetric and simulated compact polarimetric parameters to monitor soil moisture and freeze/thaw state in southwest Ontario". This paper is to be submitted to the international journal *Remote Sensing of Environment* in April 2015. Finally, the thesis concludes in Chapter 4 with a

summary of the research and a further discussion of results and limitations of the research plus a

suggestion of future research areas.

Chapter 2

Background Review

2.1 Microwave Remote Sensing Basics

Microwave remote sensing observations use the microwave portion of the electromagnetic spectrum, where the frequencies range from 0.3 to 300 GHz (1 m to 1 mm in wavelength) (Ulaby et al., 1981). The wavelengths are much longer than those of the visible and infrared part of the spectrum. This enables microwave signals, especially at low frequencies, to penetrate cloud cover without atmospheric interference. The effect of rain is negligible when the wavelength exceeds 4 cm (Ulaby et al., 1981). In addition, active microwave sensors utilize their own source of illumination rather than relying on the sun. Therefore, active microwave systems operate in all-weather conditions and during day or night. Microwaves of different frequencies can also penetrate vegetation canopies and very dry soils to various depths, thus providing volumetric and sub-surface information (Richards, 2009). Moreover, features on the Earth's surface appear differently in the microwave spectrum compared to the optical spectrum (eg. visible and infrared region) because the electromagnetic energy scattering processes are different (Ulaby et al., 1981). Thus, microwave remote sensing provides information about the target features complementary to optical remote sensing.

SAR, an active microwave sensor, transmits energy at microwave wavelengths and records the amount of energy backscattered from the terrain (Ulaby et al., 1981). Several satellite SAR sensors, such as ALOS-PALSAR, ERS, ENVISAT, RADARSAT, TerraSAR-X and SMAP,

have been launched to provide valuable information for land applications by acquiring images at different frequencies, polarizations and spatial resolution. The RADARSAT-2 satellite operates at the C-band frequency of 5.405 GHz and is capable of acquiring images at various beam modes with different swath widths, spatial resolution, incidence angles and polarizations (Canadian Space Agency, 2011). RCM is a C-band satellite constellation operating at the frequency of 5.405 GHz, which is the same as the RADARSAT-2 satellite instrument (Canadian Space Agency, 2011). The baseline mission includes three satellites, but the constellation is designed to be scalable to six satellites to meet future data demands. The RCM greatly improves the temporal resolution with an average of daily global re-look and a four-day exact revisit capabilities (Canadian Space Agency, 2013). The mission also includes the CP mode in the system design which can acquire images at wider swaths while maintaining rich information content (Charbonneau et al., 2010), which is a huge advantage over other SAR modes, such as single/dual polarimetry and QP. Detailed discussion of different radar modes is presented in **Section 2.2**.

2.2 Radar Systems

Radar technology has gained considerable importance since 1980s and has become a focus of research activities (Zebker et al., 1987). Several space-borne and air-borne SAR systems have been developed and deployed. Traditional systems are single polarimetric (SP) and DP instruments with more sophisticated ones being QP system. CP is relatively new and has only been investigated in recent years. This section provides a detailed description of the key radar systems mentioned above for remote sensing applications.

2.2.1 Single and Dual Polarimetry

The SP system transmits and receives only one polarization, H or V. The conventional DP system transmits in one linear polarization and receives in two, i.e. (HH, HV), (VH, VV) or (HH, VV) (Shirvany et al., 2013). These two radar configurations are straightforward to implement, but they only capture partial polarimetric information about the target, plus the phase information is not retained during processing.

2.2.2 Quad Polarimetry

The QP system transmits horizontal and vertical polarizations alternatively and receives signals in both polarizations (HH, HV, VH, and VV). As shown in **Figure 2.1**, the ranging pulse on one polarization is transmitted first, and both horizontal and vertical polarizations are received before the transmission of the next ranging pulse on the orthogonal polarization (Richards, 2009). The QP system is expected to provide the most information about the target feature since it records the full scattering matrix of the target. It offers significant environmental insight for many applications even though the system is disadvantaged by reduced swath width, increased complexity of the radar system, and higher power required for the transmitter (Charbonneau et al., 2010).
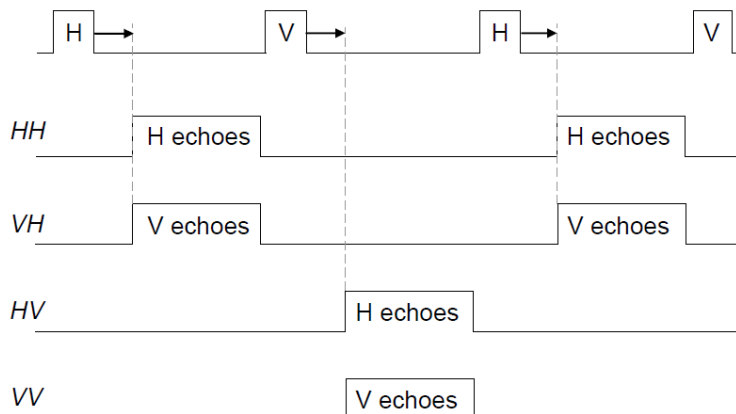
Figure 2.1 The sequence of transmitted ranging pulses and received echoes in a QP imaging radar system. (Source: Richards, 2009)

2.2.3 Compact Polarimetry

CP is essentially a DP system, which transmits one polarization and receives two (Nord et al., 2009). It gains much attention in recent years since it is able to acquire data with wider swath and reduced complexity, cost and energy requirement of the radar system while maintaining the information content of the acquired imagery (Raney, 2007). Much effort has been made to investigate the CP system as a possible alternative of the QP system. Three CP operation modes have been introduced in literature and are summarized below.

$\pi/4$ Mode

Souyris et al. (2005) proposed the $\pi/4$ mode, which transmits a linear polarization oriented at 45° with respect to the horizontal or vertical polarization and receives both horizontal and vertical polarizations. The results indicated that the $\pi/4$ mode has successfully classified crops and forests at the L-band. The $\pi/4$ mode is most successful when discriminating targets are oriented horizontally and vertically relative to the incident waves. However, many man-made objects are neither horizontally nor vertically oriented. Thus, the $\pi/4$ mode is not suitable for urban applications.

Dual Circular Polarimetric Mode

The dual circular polarimetric (DCP) mode is an alternative compact polarimetric approach introduced by Stacy and Preiss (2006), which transmits right (or left) circular polarization and receives both right and left circular polarizations (RR and RL). Pure circular polarization occurs when the horizontal and vertical polarizations with the same amplitude (i.e. power density) are transmitted simultaneously while the phase difference between them is 90° (Richards, 2009). In the case of left circular polarization as illustrated in **Figure 2.2**, the vertical

component leads the horizontal component with a positive phase angle of 90°. The total field

vector rotates in the counter-clockwise direction when viewing behind the illuminating source

and in the direction of propagation. For the right circular polarization, the vertical component

lags behind the horizontal component, and the phase angle between the two orthogonal

components is −90°. The total field vector rotates in the clockwise direction when viewing in the

direction of propagation. In addition, the circular polarization is rotational invariant. Therefore, it

is able to classify the dihedral-like objects regardless of their orientations (Raney, 2007).
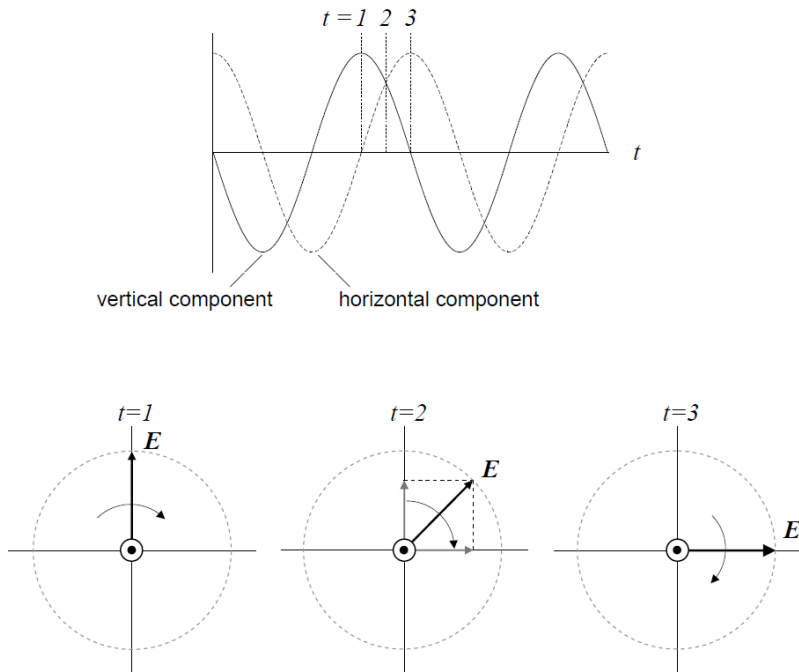
Figure 2.2 Illustration of the electric field vector rotation for left circular polarized wave.
(Source: Richards, 2009)

Circular Transmit Linear Receive Mode

Raney (2007) presented a circular-linear polarimetric (CL-pol) approach, which transmits

right circular polarization and receives both horizontal and vertical components (RH, RV). This

CL-pol configuration is also referred to hybrid polarity. Recently, the CL-pol mode has been

added to the system design of the RCM. The CL-pol architecture is relatively simple to

implement, less susceptible to noise, carrying self-calibration features, and most importantly, enabling larger swath coverage and incident angle range compared to the QP system (Charbonneau et al., 2010). The DCP mode described previously is a viable alternative to the CL-pol system, but the CL-pol configuration has simpler hardware requirement and is more straightforward to implement (Raney, 2007). The CL-pol parameters can be easily synthesized from the existing quad polarimetric images. Thus, investigation on the CL-pol configuration and benefits of this new radar architecture can be conducted without additional data collection campaigns. This is a significant aim of this thesis.

2.3 Radar Remote Sensing of Soil

Upon contact with the surface, the incident energy may be absorbed (attenuated), scattered, reflected or penetrate into the medium. The amount of energy backscattered from a surface is dependent on the radar configuration and surface properties. Properties comprising these components are explored to provide better understanding of the interaction between the active microwave signals and the terrain.

2.3.1 Physical Properties of Soil

There are two main soil properties that affect the radar backscattered energy: dielectric properties of soil which is highly dependent on its moisture content and surface roughness. A detailed discussion of these two properties is presented below.

Complex Relative Permittivity

The complex relative permittivity ϵ_r of a material is one of its electromagnetic properties, which measures the ability of a material to conduct electrical energy (Jensen, 2007). It is the ratio

of ϵ_r of a material to ϵ_r of the free space. ϵ_r is composed of a real part ϵ_r' and an imaginary part ϵ_r'' (Hoekstra and Delaney, 1974; Ulaby et al, 1981; Woodhouse, 2006):

$$\epsilon_r = \epsilon_r' + j\epsilon_r'' \qquad (2.1)$$

where $j = \sqrt{-1}$. ϵ_r' is often referred to the dielectric constant of a material (Woodhouse, 2006), while ϵ_r'' accounts for the energy lost to the material, mostly due to its moisture content (Richards, 2009).

ϵ_r of soil is principally controlled by four components: bulk soil, air, bound water and free water (Hallikainen et al, 1985). The bound water is tightly held by the soil particles, whereas the free water can move within the soil with relative ease (Hallikainen et al, 1985). The amount of bound water within the soil is directly proportional to the soil surface area, which is dependent upon the amount, shape and size of the soil particles. For example, clay soils are able to hold more bound water than sandy soils since clay soils possess larger surface area (Schmugge, 1985). Across the microwave region, liquid water (i.e. free water) has ϵ_r' approximately 80 compared to 3 to 5 for dry soils (Schmugge, 1985; Woodhouse, 2006). The large contrast between the two dielectric properties makes microwave remote sensing an effective tool for soil moisture applications. The large ϵ_r' of water results from the fact that the polar molecules can easily rotate along the direction of an applied electric field (Schmugge, 1985; Richards, 2008). Anything that inhibits the rotational motion of the dipole will reduce ϵ_r' (Schmugge, 1985). When the frequency becomes higher, the water molecules can no longer keep up with the field. For example, at the frequency of infrared and visible light, the rotational response ceases and the vibrational response of the molecule and electron cloud becomes dominant (Richards, 2008). As a result, the influence on the field is much smaller and ϵ_r' of water is also smaller.

Bound water and free water have different dielectric properties. When adding water to dry soils, the ϵ_r' increases slowly as most of the water molecules are tightly bound to the surface of soil particles. The water dipoles are immobilized so that they cannot interact with the radar signal (Kornelsen and Coulibaly, 2013). As more water is added, the water molecules are further away from the soil particles' surface and are freer to rotate, thus contributing a larger amount to ϵ_r' of soils (Schmugge, 1985). In terms of ϵ_r'', it increases as the soil moisture content increases, but at a lower rate compared to ϵ_r' (Woodhouse, 2006). Ice has ϵ_r' of 3.2 (Schmugge, 1985), which is similar to that of dry soils. Thus, we can expect that ϵ_r' drops dramatically when soil water freezes. Changes in the proportion of liquid water and ice within the soil will have significant impacts on its dielectric properties. There is still free water in soils at temperature of $-24°C$ (Hallikainen et al, 1985) or even at $-40°C$ to $-50°C$ (Anderson and Tice, 1971). Thus, ϵ_r' of frozen soils is expected to be a bit higher than that of ice or dry soils. In conclusion, the dielectric properties of soil are dependent on water content, electromagnetic frequency, and temperature.

Soil Moisture Content

The spaces between the solid particles are typically fully or partially filled with water unless the soils are dry. Soil water can be pulled down by gravity, but is also attracted to the soil surface due to the electrostatic forces binding dipole water molecules to the electrically charged surfaces of solid soil particles (Hendriks, 2010). Soil can retain water for substantial periods of time so that the plant roots can extract water to survive. The quantity of water in soil can be expressed as the volumetric water content m_v (Ulaby et al, 1986):

$$m_v = \frac{V_w}{V_t} (\times 100\%) \qquad (2.2)$$

where V_w is the volume of water and V_t is the total volume of soil. The values of m_v can be fraction ($0 \leq m_v \leq 1$) or percentage ($0 \leq m_v \leq 100\%$). Gravimetric moisture m_g is another term to characterize the soil moisture content (Ulaby et al, 1986):

$$m_g = \frac{W_w}{W_{dry}} (\times 100\%) \tag{2.3}$$

where W_w is the weight of the water in the soil sample and W_{dry} is the weight of the dry soil sample. m_v is usually used to represent the soil moisture content because the dielectric mixture models are based on the volume fractions of the constituent components rather than on their weight fractions (Dobson and Ulaby, 1998).

Since ϵ_r of soil depends on its moisture content as discussed in the previous section, changes in soil moisture content can result in large variations of radar response. Empirical studies demonstrated the sensitivity of radar backscatter to soil moisture content when m_v is between 5% and 35% (Bruckler et al., 1988; Holah et al., 2005; Baghdadi et al., 2006). When the soil moisture content is higher, the radar backscatter is stronger and the surface scattering is the dominant mechanism taking place. The incident energy cannot penetrate the soil volume to a greater depth. The amount of penetration increases as the soil dries and the backscattered energy returned to the radar sensor is weaker (Richards, 2009).

Surface Roughness

The surface roughness characterization of soils is dependent on the microwave frequency, incidence angle and the surface physical characteristics. According to the Rayleigh criterion, a surface is considered smooth if

$$h < \frac{\lambda}{8 \cos \theta} \tag{2.4}$$

where h is the root mean square (RMS) height, λ is the wavelength, and θ is the incidence angle

(Ulaby et al., 1982). The modified Rayleigh criterion categorizes the level of roughness into

smooth, intermediate and rough surfaces. It considers a surface smooth where

$$h < \frac{\lambda}{25 \sin \gamma} \tag{2.5}$$

and rough where

$$h > \frac{\lambda}{4.4 \sin \gamma} \tag{2.6}$$

where γ is the depression angle (Jensen, 2007). The surfaces with RMS values between the

above two criterion have an intermediate surface roughness. **Table 2.1** lists the range of RMS

heights for smooth, intermediate and rough surfaces with respect to the C-band RADARSAT-2

wavelength at various incidence angles. As the incidence angles increase, a surface with larger

RMS values is considered a rough surface.

Table 2.1 Modified Rayleigh surface roughness criteria for C-band RADARSAT-2 ($\lambda = 5.5\ cm$) at various incidence angles.

Incidence Angle (°)	Surface Roughness Category		
	Smooth (cm)	Intermediate (cm)	Rough (cm)
10°	$h < 0.225$	$0.225 \leq h \leq 1.280$	$h > 1.280$
20°	$h < 0.236$	$0.236 \leq h \leq 1.341$	$h > 1.341$
30°	$h < 0.256$	$0.256 \leq h \leq 1.456$	$h > 1.456$
40°	$h < 0.290$	$0.290 \leq h \leq 1.646$	$h > 1.646$
50°	$h < 0.345$	$0.345 \leq h \leq 1.961$	$h > 1.961$
60°	$h < 0.444$	$0.444 \leq h \leq 2.521$	$h > 2.521$
70°	$h < 0.649$	$0.649 \leq h \leq 3.686$	$h > 3.686$

As shown in **Figure 2.3a**, smooth surface acts as a specular reflector, where most of the

energy bounces off the terrain away from the antenna (Jensen, 2007). Little backscatter is

returned to the radar antenna and result in a dark tone on the radar image. As the roughness of a

surface increases (**Figure 2.3b**), there will be more backscatter energy returned to the radar

sensor and the radar image will appear in a brighter tone. A very rough surface will produce very diffuse backscatter (**Figure 2.3c**). It will produce a bright return on the radar image due to the large amount of microwave energy reflected back toward the antenna (Jensen, 2007).

a) Smooth surface   b) Intermediate surface   c) very rough surface
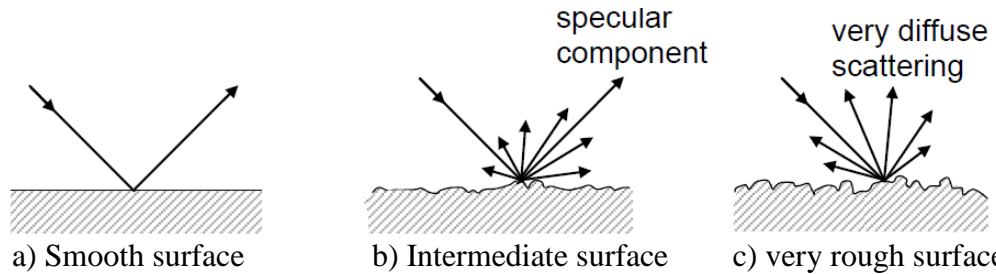
Figure 2.3 Expected radar backscatter from different levels of surface roughness. (Source: Jensen, 2007)

2.3.2 Radar Properties

Three properties of the radar have the greatest influence on the backscattered energy received by the sensor: frequency, polarization and incident angle. Each presents varying influences to target interaction and they are discussed with respect to soil moisture applications in this section.

Frequency

Frequency is important for understanding how the radar signals interact with a target feature. A given surface will appear differently at different frequencies. For example, a smooth surface for C-band microwaves may appear rough for X-band microwaves, thereby producing different image tones and backscatter values at the two frequencies. Frequencies of incident waves directly influence the penetration depth (Ulaby et al., 1982), as illustrated in **Figure 2.4**. For soils with the same moisture level, lower frequency such as L-band (1 GHz – 2 GHz) has the greatest penetration depth, followed by the C-band (4 GHz – 8 GHz) and X-band (8 GHz – 12 GHz). The penetration depth decreases as the soil moisture content increases. Empirical results

of Bruckler et al. (1988) showed that the penetration depth of the C-band (4.5 GHz) HH polarization at the incidence angle of 15° for a clay loam soil decreases from 5 cm with soil moisture content of 10% to about 1 cm with soil moisture content of 30%. Thus, C-band radar can be used to detect the near-surface soil moisture content and state. In addition, studies have demonstrated that dry snow is virtually transparent for the C-band waves (Pivot, 2012; Bernier and Fortin, 1998). Therefore, the ground conditions can be retrieved during the winter often independent of any snow cover.
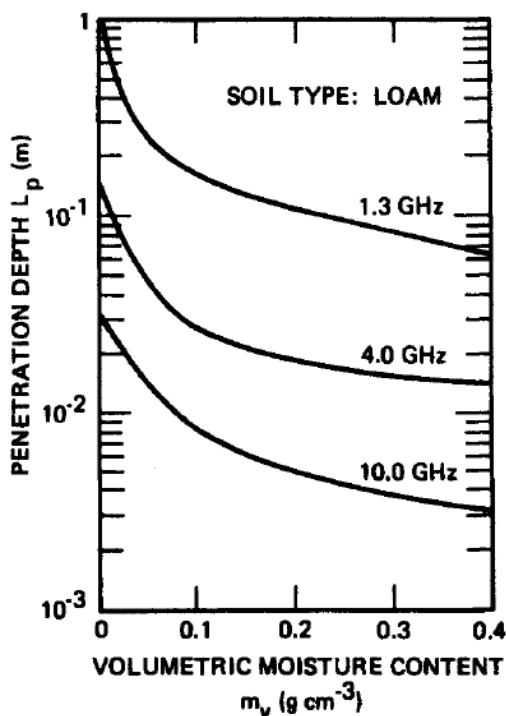
Figure 2.4 Penetration depth as a function of frequency for loam soils. (Source: Ulaby et al., 1982)

Polarization

The horizontal and vertical polarized waves are most sensitive to features with a similar structural alignment (Raney, 1998). HH is more sensitive to soil properties as the horizontally polarized microwaves can penetrate the vegetation canopy more easily, thus minimizing impacts of vertical stalks and providing more information about the underlying soil conditions (McNairn

17

and Brisco, 2004). On the other hand, the vertically polarized microwave is more sensitive to targets with a strong vertical component. Since the penetration of vertically polarized microwaves through the vegetation canopy is less, VV polarization can detect the differences within the vertical vegetation structure from various growth stages (McNairn and Brisco, 2004). Baronti et al. (1995) reported that σ_{HH}^0 should be approximately equal to σ_{VV}^0 for bare soils at C-band where surface scattering dominates and σ_{VV}^0 would be smaller with the presence of crop stalks as σ_{VV}^0 is attenuated within the vegetation canopy. Therefore, the HH polarization is most often recommended for soil moisture studies with minimum influence of vegetation.

The cross-polarized radar returns (i.e. HV and VH) result from multiple or volume scattering from very rough surfaces and vegetation canopy. They provide complementary information about the crop structure within the canopy (McNairn and Brisco, 2004). The cross-polarized backscatter measurements would increase significantly when the incident waves interact with vegetation volume (Baronti et al., 1995).

In terms of the circular polarizations, RL results from smooth surfaces with dominance of surface scattering (Evans et al., 1988; Raney, 2007). Volume or multiple scattering changes the handedness of the incident circular waves relative to the observer, which produces RR polarization (McNairn and Brisco, 2004). Baronti et al. (1995) found that σ_{RL}^0 should be much greater than σ_{RR}^0 when surface scattering dominates, and σ_{RR}^0 would increase considerably and should be approximately equal when the volume scattering component is larger.

Incidence Angle

In general, backscatter decreases with larger incidence angles since the surface appears smoother as the incidence angles increase (See **Section 2.3.1** surface roughness section for more details). When surface roughness increases, the dependence on incidence angle is weaker, while

for smoother surfaces there is a strong dependence (Ford, 1990). As shown in **Figure 2.5**, at low

incidence angles (i.e. $< 30°$), the change of incidence angle can result in large changes of radar

backscatter. The influence of surface roughness is relatively small at this range. For example,

when changing from intermediate to rough surfaces, the impact on the radar backscatter is very

small for incidence angles of $20° - 25°$. In the range of incidence angles between $30°$ and $60°$,

the changes in surface roughness have a bigger impact on radar backscatter compared to the

changes in incidence angle. At incidence angles greater than $60°$, radar backscatter is low and

surfaces appear dark in images relative to low-incidence-angle observations.

     Therefore, low incidence angles ($< 30°$) are the most optimal for soil moisture estimation

with a minimum influence of soil surface roughness. Several studies have demonstrated that

radar backscatter has the highest sensitivity to soil moisture at steep incidence angles and

variations of surface roughness can be better characterized by radar backscatter at high incidence

angles ($40° - 50°$) (Baghdadi et al., 2002; Holah et al., 2005; Adams et al., 2013).
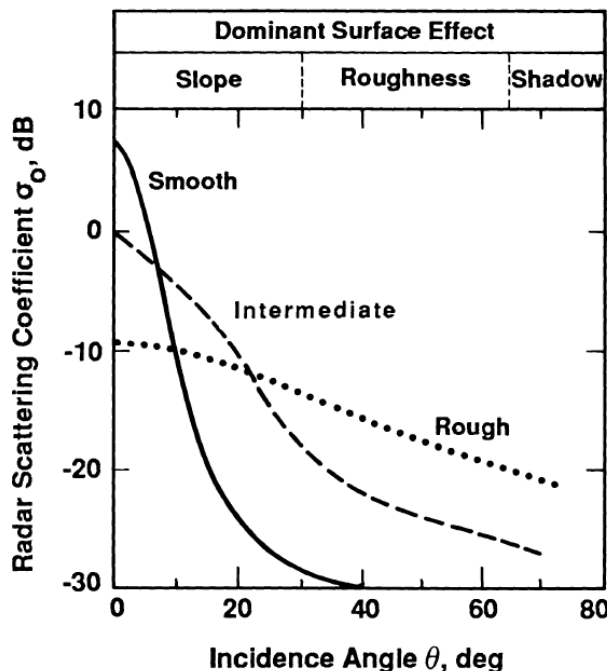
Figure 2.5 Effect of surface roughness on radar backscatter at different incidence angles (Source: Ford, 1990).

2.3.3 Scattering Mechanisms

Radar scattering from a target is strongly affected by the surface geometrical properties. The most commonly used scattering mechanisms in agricultural applications to decompose radar backscatter include surface, double-bounce and volume scattering (Baronti et al., 1995; McNairn et al., 2002; Adams et al., 2013), as illustrated in **Figure 2.6**. Surface scattering occurs when a single reflection of an incident radar signal bounces back to the sensor from an object (Richards, 2009). Surface scattering prevails in areas with relatively smooth surfaces, such as bare agricultural fields. When a circular polarization is transmitted, the reverse handedness of circular polarization is received for the single-bounce scattering (Raney, 2007). For example, transmitting a right circular polarization (R) would expect to receive left circular polarization (L) for surface scattering, resulting in a RL image.

The double-bounce scattering is caused by scattering from a dihedral corner reflector, where a wave bounces between two reflector surfaces oriented orthogonally at a right angle and returns to the antenna (Adams et al., 2013). Corn stalks, tree trunks and human-made structures like buildings usually exhibit double-bounce scattering. The double-bounce scatter imposes an even number of phase reversals in the two orthogonal linear components of a wave, thus the same-sense circular polarizations are returned (Raney, 2007). For example, right circular polarization would be received when transmitting the right circular polarization, thus a RR image. The phase of the received signals from a double-bounce scatterer would differ by 180° relative to that from a single-bounce scatterer.

Volume scattering results from multiple scattering events. It occurs in the dense vegetation (McNairn et al., 2002) or in dry soils where pockets of air are present (Jackson et al., 1992). The polarimetric response from volume scattering contains a large unpolarized

component, thus decreased degree of polarization and increased randomness in phase (McNairn et al., 2002).

a) Surface scattering   b) Double-bounce scattering   c) Volume scattering
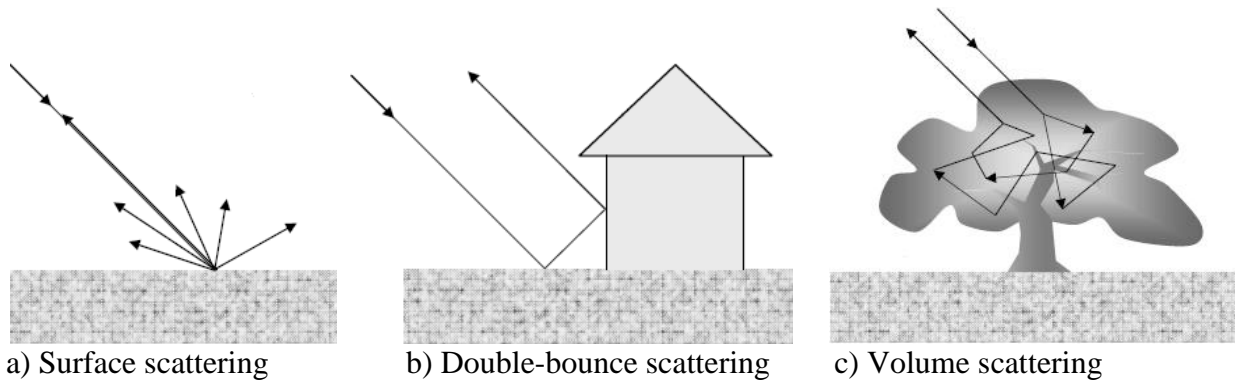
Figure 2.6 Common scattering mechanisms. (Source: Richards, 2009)

Chapter 3

The Potential of Using RADARSAT-2 Quad Polarimetric and Simulated Compact Polarimetric Parameters to Monitor Soil Moisture and Freeze/Thaw State in Southwest Ontario

Overview

The objective of this study is to assess the potential of the C-band RADARSAT-2 quad polarimetric (QP) and simulated compact polarimetric (CP) parameters to monitor soil moisture and freeze/thaw state. The study used 15 RADARSAT-2 fine QP images acquired from October 2013 to June 2014 and field measurements collected coincidentally with the radar imagery acquisitions. The CP images were simulated from the acquired RADARSAT-2 QP images. All linear and circular radar backscatter responses were able to discriminate between frozen and unfrozen soils. But their correlations with soil moisture content were weak within each group. The Oh model was implemented in this study to compare with acquired RADARSAT-2 data and to confirm our understanding of the radar response from soil. A good agreement was found between the backscattering coefficients simulated by the Oh model and the RADARSAT-2 data, indicating that the C-band radar backscatter can detect the near-surface soil moisture and state and the study site with 4-inch tall standing hay stalks behaved similarly as a bare soil site at the C-band. The study did not show statistically significant correlation between CP parameters and soil moisture content if examining frozen and unfrozen soils separately. But the results

demonstrated that the first and fourth Stokes parameters and $m - \delta$ surface and volume

scattering components were sensitive to soil freeze/thaw state. It suggested that the CP mode can

be an alternative data source for large-scale C-band frozen/unfrozen soils mapping. More image

acquisitions during the freezing and thawing periods, complete continuous field measurements of

soil moisture and state, and ground measurements over wide areas can provide better knowledge

of soil freezing and thawing processes and help further develop understanding of the CP

parameters, thus facilitating future use of the CP mode.

3.1 Introduction

Soil moisture is a key state variable in many hydrological and meteorological

applications. Hydrologically, it serves as a reservoir of water and drives the processes of

infiltration and surface runoff (Dingman, 2002). Infiltration determines the amount of water

available for vegetation growth and runoff has a strong impact on the rate of soil erosion and

river processes (Ulén, 2003; Hendriks, 2010). Soil moisture also plays a key role in both water

and energy cycles by influencing the energy budget at the surface/atmosphere interface through

evapotranspiration, thereby having a significant impact on the Earth's climate system (Sellers et

al., 1997). Frozen soil affects the decomposition of organic substances and the biota living in the

soil (Niu and Yang, 2006). It reduces the soil permeability and has great potential for soil erosion

during spring thaw (Hillard et al., 2003). Therefore, it is hydrologically and meteorologically

important to have accurate and timely soil moisture and freeze/thaw measurements.

Radar remote sensing offers a promising approach for monitoring near-surface soil

properties. Radar backscatter responses are influenced by the dielectric properties of soil, which

are dependent on the water and ice content (Hallikainen et al., 1985; Schmugge, 1985; Dobson

and Ulaby, 1986). Microwave imaging sensors, such as synthetic aperture radar (SAR), use their

own source of illumination which enables all-weather monitoring of the Earth surface at high

spatial resolution (i.e. meters to tens of meters) (Ulaby et al., 1981; Richards, 2009). In addition,

the C-band SAR signals can penetrate dry snow (Bernier and Fortin, 1998; Pivot, 2012), thus

providing an opportunity to observe the underlying soil conditions during the winter. The

RADARSAT-2 satellite is capable of acquiring fully polarimetric C-band backscatter

observations of the Earth at all four polarization states, i.e. HH, HV, VH and VV. The quad

polarimetric (QP) system is expected to provide the most information about the target feature

since it records the complete characterization of the scattering behavior from a target

(Charbonneau et al., 2010). Studies demonstrated that the polarimetric variables and scattering

decompositions derived from the QP data have successfully characterized agricultural surface

state (McNairn et al., 2002; Gherboudj et al., 2011; Adams et al., 2013). However, the QP

system is disadvantaged by narrow swath width, increased complexity of the radar system, and

high power requirement for the transmitter (Charbonneau et al., 2010). Despite these issues, the

rich information content makes QP a valuable data source for many applications.

The compact polarimetry (CP) approach has gained much attention in recent years since

it is able to observe the Earth with wide swath but with reduced instrument complexity, cost and

energy requirements of the radar system while maintaining the high information content of the

acquired imagery (Raney, 2007). Much effort has been made to investigate the CP system as a

possible alternative to the QP system. Three CP operation modes have been introduced in

literature: 1) π/4 mode, which transmits a linear polarization oriented at 45° with respect to the

horizontal or vertical polarization and receives both horizontal and vertical polarizations (Souyris

et al., 2005); 2) dual circular polarimetric mode, which transmits right (or left) circular

polarization and receives both right and left circular polarizations (Stacy and Preiss, 2006); 3) circular-linear polarimetric (CL-pol) mode, also refers to hybrid polarity, which transmits right circular polarization and receives both horizontal and vertical components (Raney, 2007). The CL-pol mode has been added to the system design of the Canadian RADARSAT Constellation Mission (RCM), which is planned for launch in 2018 (Canadian Space Agency, 2013). However, very few studies on soil moisture and freeze/thaw conditions using the CP data have been conducted, and more research is needed to further investigate the new CP mode and support the future satellite mission.

The aim of this study, therefore, is to evaluate the sensitivity of RADARSAT-2 QP and simulated CP parameters to soil moisture and freeze/thaw state over an agricultural site in southwest Ontario, Canada. The following specific objectives were set to achieve this aim. First, RADARSAT-2 QP backscatter observations were acquired along with coincident ground measurements of soil moisture content and state to enable us to characterize the physical nature of the study domain. Second, implementation of the Oh et al. (1992) model backscatter estimates of bare inorganic soils confirmed our understanding of the radar responses. Third, with the established remote sensing and hydrologic knowledge, the CP parameters were then investigated to assess their utility in monitoring the changes of soil moisture and state over time.

3.2 Study Area

The study site is a hay field located within the Strawberry Creek catchment, a small watershed in the Grand River basin. Strawberry Creek is a two-kilometer long first-order stream. It drains southeast into Hopewell Creek, and eventually discharges to Lake Erie via the Grand River. The site is approximately 15 kilometers northeast of the City of Waterloo, Ontario,

25

Canada (**Figure 3.1**). The size of the study area is about 9 hectares. The field was harvested in

early October 2013, leaving 4-inch tall standing hay throughout the study period (**Figure 3.2b**).

The study site consists of two soil types: Guelph loam and Maryhill loam, as illustrated in

Figure 3.2a. They both have relatively good water-holding capacity, good natural supply of

plant nutrients and are high in agricultural productivity (Presant and Wicklund, 1971).
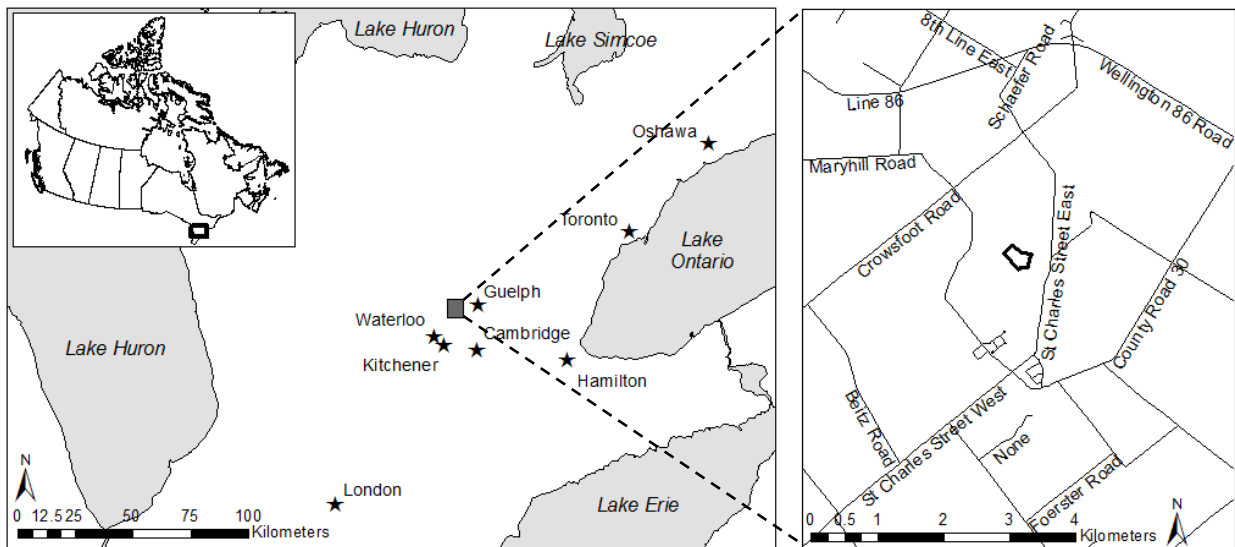
Figure 3.1 Study site location.

Figure 3.2 (a) Sampling design, soil types and meteorological station (star); (b) field photo taken on October 29th, 2013; (c) field photo taken on January 9th, 2014.

3.3 Methodology

3.3.1 Satellite Imagery

A total of 15 RADARSAT-2 fine QP images were acquired from October 2013 to June 2014 over the study area. The image acquisition dates and other characteristics were listed in **Table 3.1**. These images were provided by Canadian Space Agency through the Science and Operational Applications Research – Education (SOAR-E) initiative. Studies have demonstrated that low incidence angles ($< 30°$) are the most optimal for soil moisture estimation with a minimum influence of soil surface roughness (Ulaby et al., 1978; Dobson and Ulaby, 1986; Holah et al., 2005; Baghdadi et al. 2006; Adams et al., 2013). Thus, low-incidence-angle beam modes FQ2 and FQ5 were chosen to acquire images. Swath width of the fine QP beam mode is approximately 25 kilometres. Each fine QP imagery has four channels, i.e. HH, HV, VH and VV.

The CP images were simulated using the software provided by the Canada Centre for Remote Sensing. A full description of the simulation method can be found in Charbonneau et al. (2010). A total of 11 CP parameters were simulated from each RADARSAT-2 fine QP image acquired. Stokes vector and parameters derived from the Stokes vector were evaluated in this study. A detailed description of these CP parameters is provided in **Section 3.3.4**. The RCM noise floor was set to 0 dB so that the spatial resolution of the input fine QP was reserved. The QP images were simply converted to the CP images without modification of the original data in terms of radiometry and noise level.

Table 3.1 Characteristics of RADARSAT-2 images acquired over the study area.

Acquisition Date	Beam Mode	Pass	Incidence Angle (°)	Spatial Resolution (Range × Azimuth) (m)
October 11th, 2013	FQ5	Descending	23.5 – 25.2	12.7 × 7.6
October 29th, 2013	FQ2	Ascending	20.2 – 21.9	14.6 × 7.6
November 4th, 2013	FQ5	Descending	23.5 – 25.2	12.7 × 7.6
November 22nd, 2013	FQ2	Ascending	20.2 – 21.9	14.6 × 7.6
November 28th, 2013	FQ5	Descending	23.5 – 25.2	12.7 × 7.6
January 9th, 2014	FQ2	Ascending	20.2 – 21.9	14.6 × 7.6
January 15th, 2014	FQ5	Descending	23.5 – 25.2	12.7 × 7.6
February 2nd, 2014	FQ2	Ascending	20.2 – 21.9	14.6 × 7.6
February 8th, 2014	FQ5	Descending	23.5 – 25.2	12.7 × 7.6
February 26th, 2014	FQ2	Ascending	20.2 – 21.9	14.6 × 7.6
March 4th, 2014	FQ5	Descending	23.5 – 25.2	12.7 × 7.6
March 22nd, 2014	FQ2	Ascending	20.2 – 21.9	14.6 × 7.6
April 15th, 2014	FQ2	Ascending	20.2 – 21.9	14.6 × 7.6
May 15th, 2014	FQ5	Descending	23.5 – 25.2	12.7 × 7.6
June 8th, 2014	FQ5	Descending	23.5 – 25.2	12.7 × 7.6

3.3.2 Image Processing

The RADARSAT-2 images were first imported in PCI Geomatica with sigma nought (σ^o) calibration. Multilooking was performed for both calibrated RADARSAT-2 fine QP and simulated CP images using European Space Agency's NEST software. One range and three azimuth looks were used for FQ2 images, and one range and two azimuth looks were used for FQ5 images. All the images were further smoothed using a 3 × 3 Lee filter, which was chosen because of its ability to reduce speckle noise while preserving the edge. The images were geometrically corrected using the PCI Geomatica OrthoEngine and then clipped to the study site. The parameter values were extracted for the field average and the time series and statistical analyses were performed at this averaged field scale. The study area contained approximately 300 pixels for FQ2 and 500 pixels for FQ5 images.

3.3.3 Ground Data Collection

Field measurements were collected to compare with the satellite imagery. A meteorological station was installed on site (**Figure 3.3a**) to record air temperature, precipitation, wind speed and direction, snow depth and net radiation at long and short wavelengths every 15 minutes. Two Stevens Hydra-II probes (denoted hereafter as the Hydra probe) were installed next to the weather station to provide monitoring and sampling of soil conditions at depths of 5 cm and 15 cm below the soil surface every 15 minutes (**Figure 3.3b**). The Hydra probes operate at the frequency of 50 MHz and measure the complex relative permittivity (ϵ_r' and ϵ_r'') of the soil (Stevens Water Monitoring System Inc., 2007). ϵ_r' and ϵ_r'' are used to determine the soil moisture content and electrical conductivity, respectively. The Hydra probe also measures the soil temperature. The accuracy of the relative permittivity and soil moisture measurements are ± 0.5 and $\pm 0.03\ m^3/m^3$, respectively (Stevens Water Monitoring System Inc., 2007).

Wide-area soil moisture sampling was also made across the field using a Delta-T WET sensor (**Figure 3.3c**) when the RADARSAT-2 images were acquired. The measurements were taken along a grid of equally spaced points with 30-meter interval. Similar to the Hydra probe, the Delta-T WET sensor measures ϵ_r', then calculates the soil moisture and electrical conductivity of pore water from the measured ϵ_r' (Delta-T Devices Ltd, 2005). It also measures the soil temperature and electrical conductivity of the surface soil. The Delta-T WET sensor operates at the frequency of 20 MHz and the accuracy of ϵ_r' and soil moisture measurements are ± 2.5 and $\pm 0.04\ m^3/m^3$, respectively (Delta-T Devices Ltd, 2005).

Since the relative permittivity is dependent on the frequency and the two different types of sensors operate at two different frequencies and have different range and accuracy, the measurements needed to be calibrated to ensure consistency among sensors and make the

29

measurements comparable. Calibration was done in a laboratory by adding increasing amounts of water to dry sand samples. ϵ'_r was measured by the Hydra probe and Delta-T WET sensor for each moisture level. A linear regression was derived to standardize the Delta-T sensor to the Hydra probe. For completeness, snow depth measurements were also carried out with soil moisture sampling across the field during the winter coinciding with the RADARSAT-2 overpasses (**Figure 3.3d**).

Soil roughness measurements were conducted on November 13th 2013 (before winter) and May 6th 2014 (after winter). Two roughness profiles were measured on each date, one along the north-south direction and the other one along the east-west direction. The two transects had the same centre point. The pin meter technique was used to capture the vertical variability of the ground to the reference surface. A meter ruler was placed and leveled about 20 cm above the ground. The vertical distance between the meter ruler and the ground was collected at 2 cm spacing. The root mean square (RMS) roughness value was calculated for each roughness profile using the following equation:

$$RMS = \sqrt{\frac{\Sigma(l - \bar{l})^2}{n}} \tag{3.1}$$

where l is the vertical distance between the meter ruler and the ground, $\bar{l}$ is the mean of l, and n is the number of measurements, which is 50 in this case. The t-test was run to compare the means of $(l - \bar{l})^2$ of two transects on each date. Results showed that there was no statistically significant difference between the means of the two orthogonal transects. Thus, the average RMS value of the two transects could be used to represent the field roughness for each date, as reported in **Table 3.2**. The RMS was slightly reduced during the winter, from 1.17 cm on

November 13th 2013 to 1.13 cm on May 6th 2014. The difference in RMS was considered

negligible.

Table 3.2 RMS roughness measurements collected on two dates.

Date	November 13th 2013		May 6th 2014	
Direction of Transect	North-South	East-West	North-South	East-West
RMS (cm)	1.11	1.22	1.10	1.16
RMS Average (cm)	1.17		1.13	

Figure 3.3 (a) Weather station; (b) Hydra probes installed to provide soil measurements at two depths: 5 cm and 15 cm; (c) Delta-T WET sensor used to collect soil measurements across the entire study site; (d) soil moisture and snow depth measurements were made during the winter.

3.3.4 Compact Polarimetric Parameters

Five CP parameters were examined in this study including Stokes vector, degree of polarization, circular ratio, relative phase, and $m - \delta$ feature decomposition. The four-element Stokes vector is a convenient way to describe the polarization state of the electromagnetic wave, and it is expressed as:

$$S = \begin{bmatrix} S_0 \\ S_1 \\ S_2 \\ S_3 \end{bmatrix} = \begin{bmatrix} a_H{}^2 + a_V{}^2 \\ a_H{}^2 - a_V{}^2 \\ 2a_H a_V \cos \delta \\ 2a_H a_V \sin \delta \end{bmatrix} \tag{3.2}$$

where S_0 refers to the total power received by the receiving channels, S_1 indicates the power density difference between two channels, S_2 and S_3 describe the ellipticity of the polarization, a is the amplitude of the subscripted polarization (i.e. horizontal or vertical), and δ is the relative phase (Richards, 2009). The Stokes vector for the circular-linear CP system can be expressed as:

$$\begin{bmatrix} S_0 \\ S_1 \\ S_2 \\ S_3 \end{bmatrix} = \begin{bmatrix} \langle |E_{RH}|^2 + |E_{RV}|^2 \rangle \\ \langle |E_{RH}|^2 - |E_{RV}|^2 \rangle \\ 2Re\langle E_{RH} E_{RV}^* \rangle \\ -2Im\langle E_{RH} E_{RV}^* \rangle \end{bmatrix} \tag{3.3}$$

where E is the complex voltage in the subscripted polarization, $*$ denotes complex conjugate, RH and RV are the polarizations with right-circular transmit and horizontal and vertical receive, the angle bracket $\langle ... \rangle$ denotes averaging, and Re and Im represent real and imaginary values of the complex cross-product amplitude, respectively (Raney, 2007).

Three CP parameters can be derived from the Stokes vector: degree of polarization, circular ratio, and relative phase. The degree of polarization (m) is an important parameter characterizing a partially polarized wave. It is equal to the power density of the polarized part of the wave divided by the total power density:

$$m = \frac{\sqrt{S_1{}^2 + S_2{}^2 + S_3{}^2}}{S_0{}^2} \tag{3.4}$$

where m ranges from 0 for an unpolarized wave to 1 for a completely polarized wave (Raney, 2007). The polarimetric responses from areas with dominant surface scattering have a large m due to lack of intense geometric structures. In contrast, targets with dominant multiple or volume scattering are indicative of high depolarization processes with returned signals being more random in phase. Double-bounce scattering is usually associated with a moderate m (Adams et al., 2013).

The second parameter, Circular ratio (μ_C), is the ratio between the image power in the same-sense (RR) and opposite-sense (RL) circular polarization (Raney, 2007). It can be computed as follows:

$$\mu_C = \frac{S_0 - S_3}{S_0 + S_3} \tag{3.5}$$

where $\mu_C \geq 0$. μ_C approaches to 0 for surface scattering and infinity when double-bounce scattering occurs. In the case of volume scattering, it is close to 1 or exceeds unity by a small factor (Raney, 2007).

The third parameter, relative phase (δ), is defined as the difference between the two phase angles of orthogonal (horizontal and vertical) components of the electric field vector (Li et al., 2013). It has the contribution from both linear (the third Stokes parameter S_2) and circular (the fourth Stokes parameter S_3) components:

$$\delta = atan\left(\frac{S_3}{S_2}\right) \tag{3.6}$$

where δ ranges between $-180°$ and $180°$ (Raney, 2007). δ of the right and left circular

polarizations are $-90°$ and $90°$, respectively. Linear polarization has δ of $0°$. For the right-

circular transmit CP mode, the received signals from surface scattering would be left-circular

polarized and those from double-bounce scattering would be right-circular polarized. δ of the

received waves from these two events would differ by $180°$. Therefore, δ is an effective

discriminator for single- and even-bounce scattering events (Raney, 2007).

Lastly, The first Stokes component (S_0), degree of polarization (m), relative phase (δ)

were used to generate the $m - \delta$ feature decomposition basis:

$$\begin{bmatrix} V_R \\ V_G \\ V_B \end{bmatrix} = \begin{bmatrix} \sqrt{S_0 m \dfrac{(1 - \sin\delta)}{2}} \\ \sqrt{S_0(1 - m)} \\ \sqrt{S_0 m \dfrac{(1 + \sin\delta)}{2}} \end{bmatrix} \tag{3.7}$$

where V_R, V_G, and V_B represent double-bounce, volume and surface scattering, respectively

(Charbonneau et al., 2010). The $m - \delta$ decomposition technique is similar to the decomposition

methodologies applied to the QP images, such as Freeman-Durden and Entropy−Alpha

decompositions. It has a rich potential for image interpretation and analysis (Raney, 2007).

However, it is still relatively new and further investigation is required.

3.3.5 Application of the Oh Model

The Oh model was implemented in this study to confirm our understanding of the radar

responses acquired by RADARSAT-2. The Oh model (Oh et al., 1992) established a framework

representing active microwave scattering from bare soil surfaces. An empirical relationship was

built between the radar backscatter and soil moisture content, roughness, radar incidence angle

and frequency. Two terms form the basis of the model. The first term is ks, where k is the wavenumber and s is the RMS roughness of the soil surface. The second term is ϵ_r, which is the complex relative permittivity of the soil. Oh et al. (1992) first developed two empirical equations to represent the cross-polarized ratio q and co-polarized ratio p using ks and ϵ_r:

$$q \triangleq \frac{\sigma_{hv}^o}{\sigma_{vv}^o} = 0.23\sqrt{\Gamma_o}[1 - \exp(-ks)] \tag{3.8}$$

and

$$\sqrt{p} \triangleq \sqrt{\frac{\sigma_{hh}^o}{\sigma_{vv}^o}} = 1 - \left(\frac{2\theta}{\pi}\right)^{[1/3\Gamma_o]} \exp(-ks) \tag{3.9}$$

Then, the following three equations were generated to produce σ^o estimates for three polarizations based on the cross- and co-polarized ratios obtained through **Equation 3.8 and 3.9** (Oh et al., 1992):

$$\sigma_{vv}^o(\theta, \varepsilon_r, ks) = \frac{g\cos^3\theta}{\sqrt{p}} \cdot [\Gamma_v(\theta) + \Gamma_h(\theta)] \tag{3.10}$$

and

$$\sigma_{hh}^o(\theta, \varepsilon_r, ks) = g\sqrt{p}\cos^3\theta[\Gamma_v(\theta) + \Gamma_h(\theta)] \tag{3.11}$$

and

$$\sigma_{hv}^o(\theta, \varepsilon_r, ks) = q\sigma_{vv}^o(\theta, \varepsilon_r, ks) \tag{3.12}$$

The Oh model is valid when $ks \leq 3$, $\theta \geq 20°$ for smooth surfaces and $0° \leq \theta \leq 70°$ for rough surfaces (Oh et al., 1992). In this study, $k = 113.28$ and $s = 1.15 \ cm$ (i.e. the average of all the RMS measurements), so that $ks = 1.30$. θ used in the Oh model is 22.7°, which is the average of the nominal incidence angles of FQ2 (21.05°) and FQ5 (24.35°). They are all within

the validity range of the Oh model. The complex relative permittivity (ϵ'_r and ϵ''_r) measured by the Hydra probe at both 5 cm and 15 cm below the surface was used in the Oh model to simulate radar backscatter for bare soils.

The performance of the Oh model was evaluated using the statistical indexes suggested by Willmott (1992):

$$Mean\ Bias\ Error\ (MBE) = \frac{1}{N}\sum_{i=1}^{N}(P_i - O_i) \tag{3.13}$$

$$Root\ Mean\ Square\ Error\ (RMSE) = \sqrt{\frac{1}{N}\sum_{i=1}^{N}(P_i - O_i)^2} \tag{3.14}$$

where P is the model-predicted value, O is the observed value, and N is the number of observations. Both MBE and $RMSE$ were expressed in decibels.

3.4 Results

3.4.1 Field Measurements

Figure 3.4 showed the calibration between the Hydra probe and Delta-T WET sensor. The Delta-T WET sensor tended to give a larger ϵ'_r compared to the Hydra probe when ϵ'_r reached 20 and larger. The linear regression equation displayed in **Figure 3.4** was used to adjust the WET sensor measurements to the Hydra probe. The calibrated ϵ'_r of the WET sensor was plotted in **Figure 3.5a**. The field mean and standard deviation of ϵ'_r were reported in **Table 3.3**. During the winter, the point measurements of ϵ'_r collected by the Hydra probe at 5 cm matched closely to the field measurements of ϵ'_r collected by the WET sensor. The difference of $3 - 5$ between the two sensors in fall could account for minor field variation and different ϵ'_r measurement accuracy, i.e. ± 2.5 for the WET sensor and ± 0.5 for the Hydra probe. Smaller ϵ'_r

measured by the 5 cm Hydra probe in the spring ($10 - 15$ lower than the WET sensor) might be due to the cracks formed within the soil during the freeze-thaw process and large pores caused by the melting of ice crystals (Chamberlain and Gow, 1979). Since liquid water has ϵ'_r approximately 80 compared to 1 for the air and $3 - 5$ for dry soils (Schmugge, 1985; Woodhouse, 2006), large pores will result in smaller ϵ'_r for a given volume of soil. ϵ'_r at 15 cm returned to similar levels of fall 2013 because deeper soils were not completely frozen during the winter. The crack effect of the freeze-thaw cycle on soils was less at greater depth compared to surface soils.

Both ϵ'_r and ϵ''_r were consistently higher at 15 cm depth than 5 cm over the study period. As the air temperature decreased to approximately $-15℃$ in late November (**Figure 3.5b**), ϵ'_r at 5 cm dropped below 10 while ϵ'_r at 15 cm still remained above 20. It indicated that soils started to freeze from the surface in late November and the soils at 15 cm depth were still unfrozen. The thawing and refreezing cycle in early December caused a big jump of ϵ'_r at 5 cm. ϵ'_r at 15 cm eventually dropped to around 10 in February 2014 when the air temperature reached $-30℃$. The abrupt increase of ϵ'_r at two depths in early April corresponded to the spring thaw. Soil freezing and thawing processes occurred quickly and ϵ'_r changed instantly when soils changed between frozen and thawed state. ϵ''_r at both depths were smaller during the winter and larger when soils unfroze. The change rate was more gradual compared to ϵ'_r.

Regarding the soil temperature, it fluctuated moderately compared to more abrupt change of air temperature, as shown in **Figure 3.5b**. This can be explained by the thermal properties of soil, water and air. The heat capacity of air is very small and may be neglected. The heat capacities of water ($1.0 \ cal/(cm^3 \cdot ℃)$) and soil ($0.46 \ cal/(cm^3 \cdot ℃$) for soil minerals and $0.6 \ cal/(cm^3 \cdot ℃$)for organic matter) are much higher than the air (Jury and Horton, 2004). For

37

a given volume, more energy is needed to increase the temperature for water and soils than air. Soil temperature at 5 cm responded to the air temperature more quickly compared to 15 cm depth because deeper soil was wetter. In addition, soil temperature at 5 cm reached the minimum of $-3.1°C$ in early December with shallow snow cover and was close to $0°C$ in late February when the snow depth accumulated to 45 cm in spite of very low air temperature. It indicated that snow is an excellent insulator protecting the land surface from cold winter air.
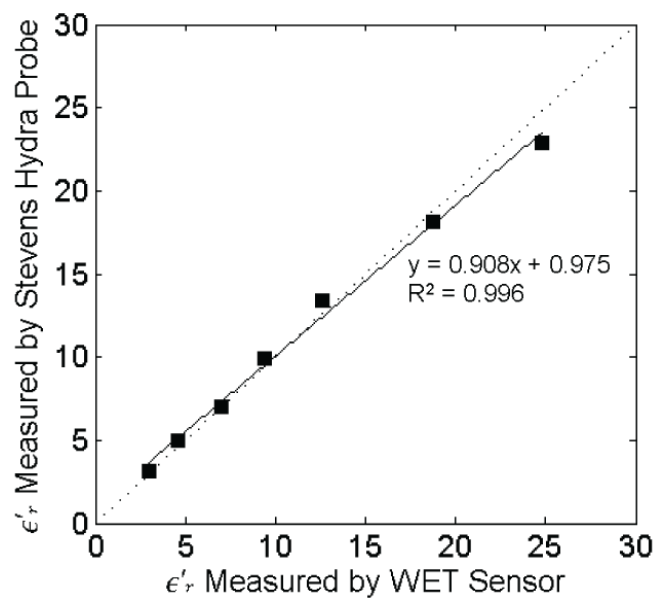
Figure 3.4 ϵ'_r of sand samples measured by the Hydra probe versus the Delta-T WET sensor for different moisture levels.
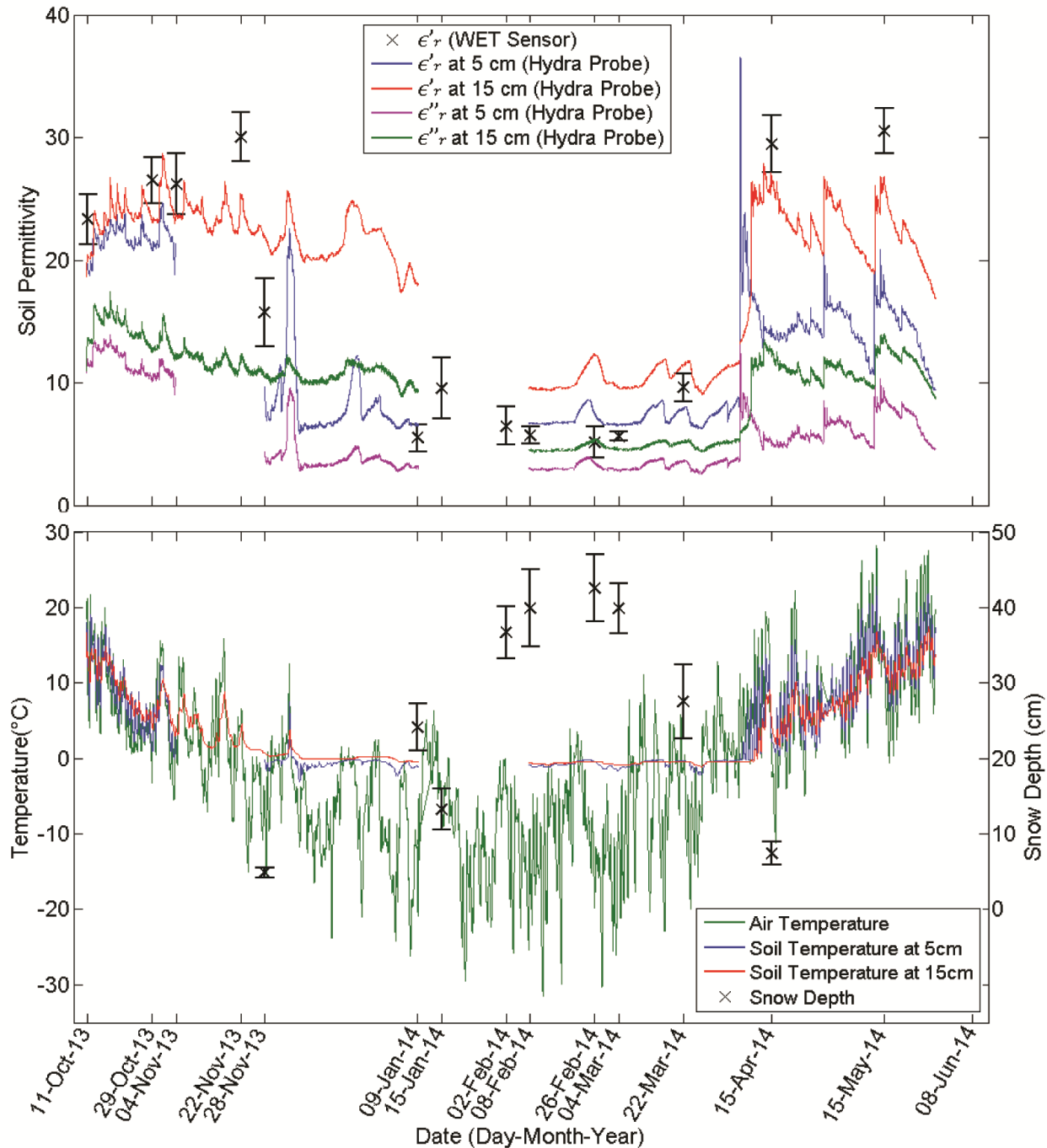
Figure 3.5 Field measurements: a) ϵ'_r measured by the WET sensor across the study site (mean $\pm$ one standard deviation) when RADARSAT-2 images were acquired and continuous ϵ'_r and ϵ''_r measurements with 15-minute interval made by the two Hydra probes installed at the field at 5 cm and 15 cm depths; b) air and soil temperature recorded by the weather station and Hydra probes with 15-minute interval and snow depths measurements collected with soil moisture sampling across the field (mean $\pm$ one standard deviation) during the winter coinciding with the RADARSAT-2 overpasses. (Note: The Hydra probe at 5 cm lost measurements between Nov 4th 2013 – Nov 28th 2013 due to connection problem and both probes lost measurements between Jan 9th 2014 – Feb 8th 2014 due to data logger defection.)

39

Table 3.3 Summary statistics of calibrated ϵ'_r of the study site collected by the WET sensor on each imagery acquisition date.

Acquisition Date	Number of Measurements	Field Mean of ϵ'_r	Standard Deviation of ϵ'_r
October 11th, 2013	69	23.3	2.0
October 29th, 2013	69	26.5	1.8
November 4th, 2013	69	26.2	2.5
November 22nd, 2013	69	30.0	2.0
November 28th, 2013	39	15.7	2.8
January 9th, 2014	5	5.5	1.1
January 15th, 2014	7	9.6	2.5
February 2nd, 2014	5	6.5	1.6
February 8th, 2014	5	5.7	0.7
February 26th, 2014	4	5.2	1.3
March 4th, 2014	4	5.6	0.4
March 22nd, 2014	5	9.6	1.1
April 15th, 2014	69	29.5	2.3
May 15th, 2014	69	30.5	1.9

3.4.2 Radar Backscattering Coefficients

The average backscatter for the study field is presented in **Figure 3.6**. Error bars represent one standard deviation either side of the mean. The like-polarization backscattering coefficients σ^o_{HH} and σ^o_{VV} exhibited similar trend during the study period, as shown in **Figure 3.6a**. They both increased approximately 1 dB from early October to early November corresponding to the increasing soil moisture content (**Figure 3.5a**) and started to decrease in late November, with a significant drop (~2 dB) on November 28th 2013 when the soil started to freeze. As the winter progressed, the radar backscatter decreased considerably due to decreased permittivity of freezing soil and vegetation. But the soil moisture measurements did not show the decreasing trend. Instead, they were relatively constant from January to early March. The backscatter reached the minimum on March 22nd 2014. Since thawing and refreezing occurred in mid-March (**Figure 3.5a**), the soil was not completely frozen and was covered with an ice layer (~1cm) on the day of image acquisition. Most of the energy was scattered away from the antenna,

resulting in low backscatter return. The sharp increase of all polarizations on April 15th 2014

corresponded to the snowmelt and thawed soils occurred before the acquisition.

The study site was covered with 4-inch tall hay stalks, which had an impact on the radar

backscatter. Baronti et al. (1995) reported that σ^o_{HH} should be approximately equal to σ^o_{VV} for

bare soils at C band. But in this study, σ^o_{VV} was lower than σ^o_{HH} in fall and spring (**Figure 3.6a**).

As the growing season started in May 2014, the vegetation height increased from 10 cm on April

15th to 25 cm on May 15th. The difference between σ^o_{HH} and σ^o_{VV} became larger and the largest

difference (~2 dB) was observed on June 8th 2014. The VV signals are more sensitive to targets

with a strong vertical component (Raney, 1998), which are the standing hay in this case.

Reduced penetration of the radar signals through the vegetation resulted in a lower backscatter

returned to the sensor for VV polarization. On the other hand, the HH waves can penetrate the

vegetation canopy to a greater extent at steep incidence angles (McNairn and Brisco, 2004), thus

a stronger backscatter for HH polarization is observed. σ^o_{VV} was reduced by 2.9 dB compared to 2

dB for σ^o_{HH} from April 15th 2014 to May 15th 2014 corresponding to the increased crop height.

The vegetation had greater influence on σ^o_{VV} compared to σ^o_{HH}. Therefore, the horizontally

polarized radar backscatter can provide more information about the underlying soil conditions,

and is more suitable for soil moisture studies with minimum influence of vegetation at steep

incidence angles.

In terms of the cross-polarization power, σ^o_{HV} and σ^o_{VH} were several orders of magnitude

lower than σ^o_{HH} and σ^o_{VV} (**Figure 3.6a**). They decreased considerably during the winter time. The

cross-polarized radar returns result from multiple or volume scattering from very rough surfaces

and vegetation canopy (McNairn and Brisco, 2004). As shown in **Figure 3.6a**, σ^o_{HV} and σ^o_{VH}

increased by approximately 3.5 dB from mid-April to early June 2014 due to increased hay

volume and height. The cross-polarizations are sensitive to the vegetation volume, thus providing information complementary to the like-polarizations.

The simulated compact polarimetric backscatter responses were very similar to the quad polarizations. σ_{RH}^o and σ_{RV}^o (**Figure 3.6b**) followed similar trend as σ_{HH}^o and σ_{VV}^o (**Figure 3.6a**), respectively. σ_{RH}^o was generally stronger than σ_{RV}^o, and a larger difference between the two polarizations was observed in fall and spring when the soil was unfrozen. σ_{RV}^o is expected to be approximately equal to σ_{RH}^o for bare soils. σ_{RL}^o was similar to the like-polarization σ_{HH}^o and σ_{VV}^o and σ_{RR}^o was similar to the cross-polarization σ_{HV}^o and σ_{VH}^o. This is expected since RL is associated with the odd-bounce reflection such as surface scattering, and RR results from double-bounce scattering (Raney, 2007). σ_{RL}^o was reduced by 2.8 dB from April 15th 2014 to May 15th 2014 compared to 2 dB for σ_{HH}^o and 1.9 dB for σ_{RH}^o corresponding to the increased crop height from 10 cm to 25 cm. It indicated σ_{RL}^o was more sensitive to the vegetation canopy than σ_{HH}^o and σ_{RH}^o. In addition, a significant increase of σ_{RR}^o was observed during the 2014 growing season. σ_{RL}^o was stronger than σ_{RR}^o by about 8 dB during the winter, but only 3.8 dB higher on May 15th and 1.5 dB on June 8th. Thus, σ_{RR}^o approached to σ_{RL}^o when there was greater contribution from vegetation.
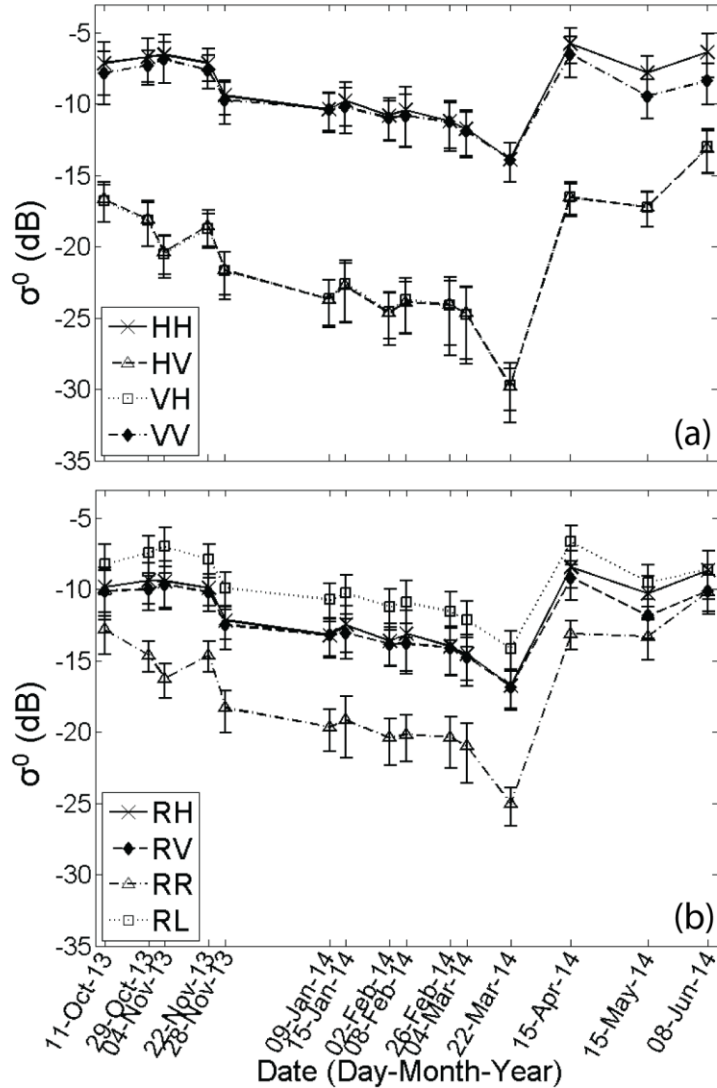
Figure 3.6 Time series of (a) RADARSAT-2 QP and (b) CP backscattering coefficients. The mean values are shown with ± one standard deviation for the entire study field.

3.4.3 Oh Model

Figure 3.7 showed very good agreement between the Oh model estimates of σ^o at 5 cm and the RADARSAT-2 observations for HH and VV polarizations. For the modeled data, σ^o_{VV} was slightly higher than σ^o_{HH} in fall the spring. But for the RADARSAT-2 data, σ^o_{VV} was generally lower than σ^o_{HH} due to the presence of hay residue and the difference between σ^o_{HH} and σ^o_{VV} became larger when the soil was unfrozen (see more detailed discussion in **Section 3.4.2**).

The Oh model also provided good estimates of σ^o for frozen soils. Overall, the study site

behaved similarly as a bare soil site at the C-band and the hay residue had minor influence to the

radar backscatter. The exception was the imagery acquired on March 22nd 2014, which had

significantly lower σ^o than the model estimates. Regarding the cross-polarization, there were

more discrepancies between the acquired and modeled data, especially when the soil was

unfrozen. Larger MBE and RMSE were observed for HV than HH and VV, as reported in **Table

3.4**. Baghdadi and Zribi (2006) and Merzouki et al. (2010) reported similar errors for all three

polarizations when comparing the model estimates to the radar observations at C-band. **Figure

3.8** showed that the Oh model estimates derived from the continuous *in situ* soil moisture point

measurements collected by the Hydra probe at 5 cm correlated well with the field mean

RADARSAT-2 backscatter. It indicated that the point measurements provided good

representation of the changes of soil moisture content and state at the field scale in this study.

The C-band radar is able to detect the near-surface soil conditions.

Table 3.4 Statistics for evaluation of the Oh model.

	HH	VV	HV
MBE	0.83	1.59	2.37
RMSE	1.72	2.04	3.61
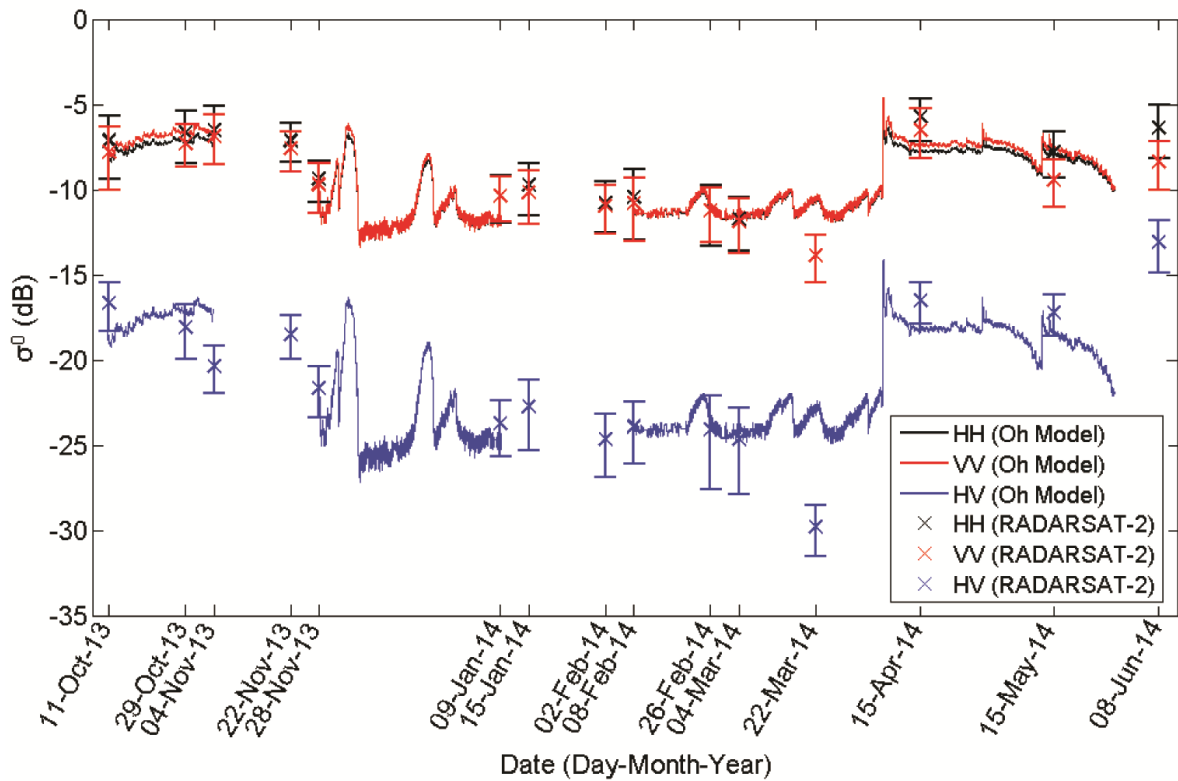
Figure 3.7 RADARSAT-2 observations and the Oh Model simulated backscatter using ϵ_r measurements of 5 cm Hydra probe. The mean values were shown with ± one standard deviation for the RADARSAT-2 backscatter. (Note: The 5 cm Hydra probe lost measurements between Nov 4th 2013 – Nov 28th 2013 due to connection problem and between Jan 9th 2014 – Feb 8th 2014 due to data logger defection.)
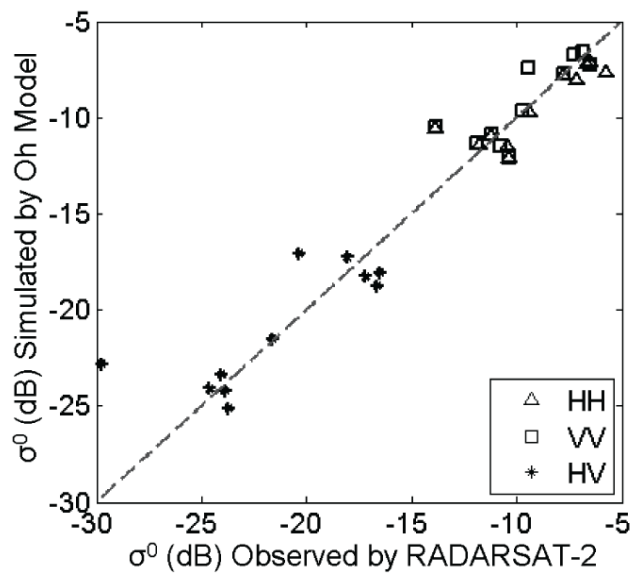
Figure 3.8 Scatterplots of the backscattering coefficients simulated by the Oh model at 5 cm vs. RADARSAT-2 data. The field mean value was used for the RADARSAT-2 data.

3.4.4 Compact Polarimetric Parameters

The mean values of the five CP parameters for the study field were presented in **Figure 3.9**. Error bars represent one standard deviation either side of the mean. In terms of the Stokes parameters, the first Stokes parameter S_0 (**Figure 3.9a**) followed the trends of σ^o_{RH} and σ^o_{RV} (**Figure 3.6b**) since it represents the total power received by the RH and RV channels, as described in **Equation 3.3**. The second Stokes parameter S_1 remained close to 0 because the power density difference between RH and RV was very small (**Figure 3.6b**). S_1 was larger when the soil thawed since RV is more sensitive to the vegetation volume and the difference between σ^o_{RH} and σ^o_{RV} was greater in fall and spring. In the case of bare soils, S_1 should be close to 0 since σ^o_{RV} should be approximately equal to σ^o_{RH}. The third Stokes parameter S_2 was also closed to 0 since S_2 describes the linear component of the radar backscatter and the received signals in this study were mostly left circular polarized with relative phase of $\pi/2$ or $90°$, as shown in **Figure 3.9b**. S_2 is equal to 0 for pure circular polarized waves (Richards, 2009). S_2 became larger in fall the spring because the increased volume scattering (**Figure 3.9c**) caused a large linear polarization component in the radar backscatter when the circularly polarized waves were transmitted (Raney, 2006). The fourth Stokes parameter S_3 varied with the shape of circular waves (Richards, 2009), and it followed the similar trend as S_0 (**Figure 3.9a**). Both S_0 and S_3 showed a clear difference between frozen and unfrozen soils. But S_3 decreased considerably when the growing season started in May 2014. S_3 decreases if the wave has a large unpolarized component and the parameter becomes 0 if the wave is linearly polarized (Richards, 2009). The volume scattering from vegetation contributes a large linear and unpolarized fraction in the received wave (McNairn et al.; 2002 Raney, 2006). As a result, S_3 was significantly lower when the proportion of volume scattering increased during the 2014 growing season (**Figure 3.9c**).

Regarding the parameters derived from the Stokes vector, as shown in **Figure 3.9b**, the relative phase δ of the received signals was approximately $\pi/2$ radians (i.e. 90°) throughout the entire study period. It indicated that the received waves were mostly left (L) circular polarized. The transmitted right (R) circular polarized wave has δ of $-\pi/2$ radians (i.e. $-90°$). The RL polarization indicated dominance of odd-bounce or surface scattering (Raney, 2007). It matched **Figure 3.9c**, which showed that the dominant component for the study site was surface scattering, followed by volume and double-bounce scatterings. δ was closer to 0 and had larger variance toward the end of the study period, indicating that the received waves contained a large linear and unpolarised component due to the influence of vegetation. The backscattered waves from volume scattering are more random in phase and contain a large unpolarized part (McNairn et al., 2002), leading to lower m in fall and spring, as show in **Figure 3.9b**. A larger m was observed during the winter due to the dominance of surface scattering. μ_C mirrored the trend of the degree of polarization. σ_{RL}^o was much larger than σ_{RR}^o during the winter when the surface scattering was dominant, thus a smaller μ_C. Greater proportion of double bounce and volume scattering in the fall and spring resulted in a smaller difference between σ_{RR}^o and σ_{RL}^o and a larger μ_C. In terms of the $m - \delta$ decomposition, the large proportion of volume and double bounce scattering component in fall the spring, as shown in **Figure 3.9c**, indicates a stronger interaction between the radar signals and the moist vegetation canopy. Another noticeable feature was that the volume scattering did not change significantly from late November 2013 to early March 2014 despite varying snow depths (**Figure 3.5b**). It confirmed that the dry snow cover was virtually transparent for C-band and matched the findings in Bernier and Fortin (1998).
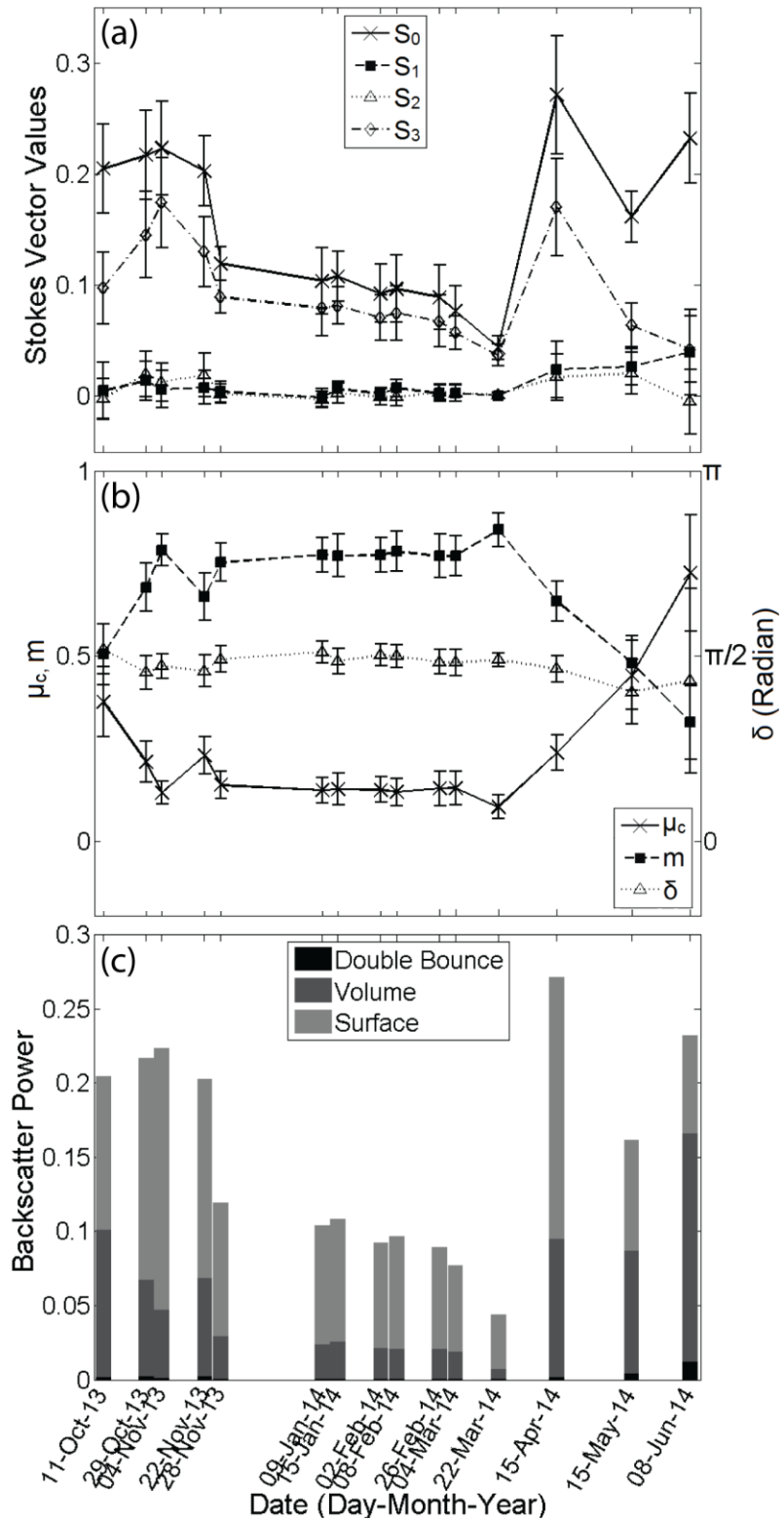
Figure 3.9 Time series of (a) Stokes vector, (b) CP parameters derived from the Stokes vector, and (c) $m - \delta$ decomposition components. The mean values are shown with ± one standard deviation for (a) and (b).

48

3.4.5 Sensitivity Analysis

The scatterplots in **Figure 3.10a** and **b** showed a clear difference of radar backscatter

over frozen and unfrozen soils and demonstrated that the C-band radar can successfully detect

freeze/thaw state of soils. Strong correlation could be expected between the backscattering

coefficients and measured ϵ_r' due to the huge contrast between frozen and unfrozen soils.

However, the high correlation coefficients are meaningless for identification of the optimal

parameters for soil moisture applications. If only considering frozen or unfrozen soils, the

correlation was weak and none of the coefficients were statistically significant, as reported in

Table 3.5. The correlation coefficients for σ_{HH}^o and σ_{VV}^o over thawed were negative, which did

not match the findings in other studies (Geng et al, 1996; Holah et al., 2005; Baghdadi et al.,

2006). This study did not demonstrate the sensitivity of C-band radar backscatter to soil moisture

content.

In terms of the Stokes parameters, **Figure 3.10c** showed that S_0 and S_3 can be used to

differentiate frozen and unfrozen soils. Similar to the radar backscattering coefficients, the

relatively large difference between frozen and unfrozen conditions could result in high

correlation coefficients. The scatterplot of S_0 was similar to that of σ_{HH}^o (**Figure 3.10a**), but the

parameter values increased exponentially when the soil thawed. The variance of S_0 and S_3 was

also larger in fall the spring compared to the winter. The correlation coefficients for both S_0 and

S_3 were negative and weak for unfrozen soils (**Table 3.5**), indicating that S_0 and S_3 are not ideal

to monitor soil water changes. S_1 and S_2 were highly correlated with ϵ_r' when soils unfroze,

suggesting that they are sensitive to soil moisture content. However, larger S_1 and S_2 values in

fall and spring resulted from greater vegetation contribution, as previously discussed in **Section

3.4.4**. The parameter values are expected to be approximately equal to 0 for bare soils where

surface scattering dominates and their corresponding correlation coefficients are also expected to be smaller.

Regarding the three parameters derived from the Stokes vector (m, μ_C and δ), δ had the highest correlation with ϵ_r' for unfrozen soils. Volume scattering from vegetation contributes a large linear and unpolarised component in the received waves (Raney, 2006), resulting in lower δ in fall and spring. Thus, δ may not be directly correlated with soil moisture content. Lastly, the $m - \delta$ surface and volume scattering components can also potentially discriminate freeze/thaw state of soils, as demonstrated in **Figure 3.10d**. But their correlation with ϵ_r' of unfrozen soils was very weak (**Table 3.5**). The $m - \delta$ double bounce scattering was positively correlated with ϵ_r' when soils unfroze. Double bounce scattering results from a wave bouncing between two reflector surfaces oriented orthogonally at a right angle (Richards, 2009), i.e. ground and hay stalks in this case. The changes of soil moisture content may not directly result in the changes of double bounce scattering. Surface scattering would be the dominant mechanism taking place for as the C-band radar signals cannot penetrate the wet soil volume to a greater depth (Ulaby et al, 1982; Bruckler et al., 1988). Therefore, surface scattering is expected to be the most correlated with soil moisture content for bare soils.

Table 3.5 Spearman correlation coefficients between ϵ_r' and SAR variables for frozen and unfrozen soils.

Variable	Frozen Soils	Unfrozen Soils
σ_{HH}^o	0.286	-0.257
σ_{HV}^o	0.143	0.029
σ_{VH}^o	0.191	0.029
σ_{VV}^o	0.286	-0.257
σ_{RH}^o	0.333	-0.429
σ_{RV}^o	0.286	-0.486
σ_{RR}^o	0.191	-0.029
σ_{RL}^o	0.286	-0.257
S_0	0.286	-0.486
S_1	0.333	0.829
S_2	-0.024	0.829
S_3	0.286	-0.371
m	0.048	-0.371
μ_C	0	0.371
δ	-0.095	-0.829
$m - \delta\ Surface$	0.286	-0.257
$m - \delta\ Double\ Bounce$	-0.238	0.600
$m - \delta\ Volume$	0.310	-0.029

* Statistically significant at p<0.05
** Statistically significant at p<0.01
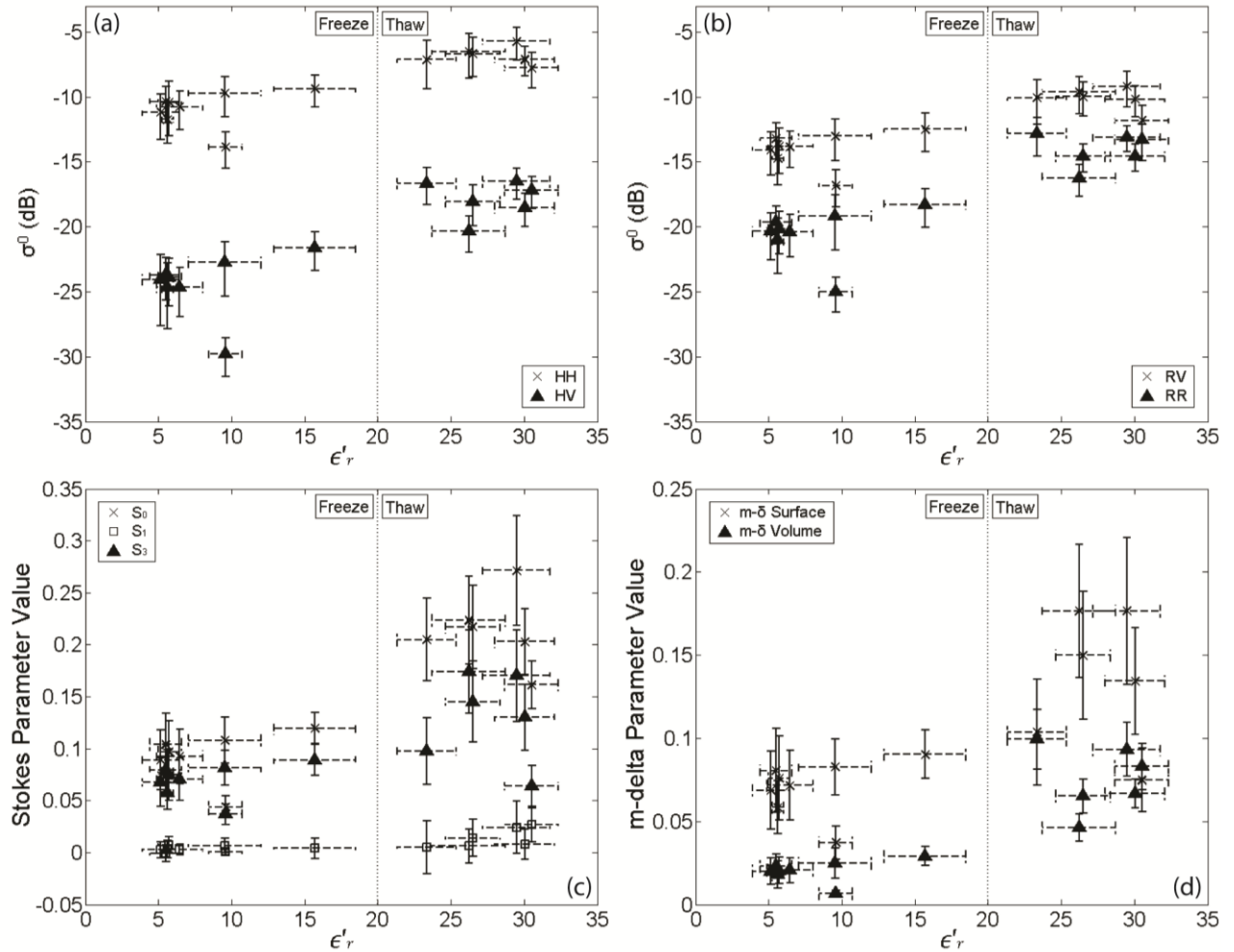
Figure 3.10 Scatterplots of selected SAR parameters vs. ϵ'_r. The mean values are shown with $\pm$ one standard deviation. Note: the freeze/thaw threshold separates the frozen and unfrozen soils based on field observations and is site specific. Soils started to freeze when ϵ'_r dropped below 20 in this study.

3.5 Discussion and Conclusions

This paper presented an exploratory and a sensitivity analysis of the C-band QP and CP variables to soil moisture and freeze/thaw state in a cold-season hydrologic environment. The radar backscatter in all polarizations can differentiate freeze/thaw state of soils, but their sensitivities to soil moisture content were relatively weak. The correlation between the C-band radar backscatter and soil moisture could be stronger at a bare field, as demonstrated in many

other studies (Geng et al., 1996; Baghdadi et al., 2006; Adams et al., 2013). The examination of linear and circular backscatter provided basic knowledge of radar responses over the study site and built confidence for the following analysis of CP parameters. The good agreement between RADARSAT-2 backscatter and Oh model estimates at 5 cm indicated that the C-band radar can detect the near-surface soil moisture content and state and the continuous *in situ* soil moisture point measurements collected by the Hydra probe provided good representation of the soil moisture at the field scale. It also demonstrated that the study site behaved similarly as a bare soil site at the C-band.

With this knowledge, the study continued to examine the CP parameters. Many of the studied CP parameters showed sensitivity to freeze/thaw state of soils, such as S_0, S_3 and $m - \delta$ surface and volume scattering components. But their correlation with soil moisture content was weak when examining frozen and unfrozen soils separately. Variables including S_1, S_2, δ, $m - \delta$ double bounce scattering were highly correlated with moisture content of unfrozen soils. However, these parameter values were more influenced by vegetation volume and their variations might not reflect soil moisture changes. This study did not build a strong case to demonstrate the sensitivity of C-band radar parameters to soil moisture changes. But it showed that the CP parameters are able to discriminate the surface soil freeze/thaw status and they can potentially be used to develop soil state classification algorithms in the future. In addition, the CP radar system could acquire data with wider swath coverage (eg. 350 km) compared to the QP system (25 km), thus facilitating large-scale frozen/unfrozen soils mapping.

One limitation of this study is that there were few images acquired during the freezing and thawing periods. It is difficult to capture freezing and thawing conditions since the soil phase change occurred quickly and ϵ'_r also responded instantly. Two clusters of points were observed

with distinct difference between the two groups, i.e. one for frozen soils and other one for unfrozen soils, which led to high correlation coefficients between pooled SAR variables and soil moisture estimates. Improved results can be obtained with more image acquisitions during the freezing and thawing periods and repetitive image coverage for additional winters. The second limitation is the Hydra probes had some missing data capturing the soil freezing process at two depths. The 5 cm Hydra probe lost measurements for the surface soil freezing in November 2013 and the 15 cm Hydra probe lost measurements for soil freezing at greater depth in January 2014. Full measurements can provide complete time series of soil moisture and state monitoring and better understanding of freezing and thawing processes. Another limitation is that only one agricultural field was examined in this study, although this was chosen to enable the study to focus on detailed knowledge of the field state. The soils of the study site have relatively good water holding capacity. The relatively small range of soil moisture content for frozen and unfrozen soils makes it difficult to examine the variability within each group. In addition, observations made from one field might not represent conditions of other areas. Thus, ground measurements over wide area with more soil types and various moisture levels can provide better representation of larger areas and help to conduct regional studies.

Despite these limitations, this study has shown promising results to detect surface soil state and qualified confidence for operational implementation of the CP data. RCM will provide an average of daily global re-look and a four-day exact revisit capabilities (Canadian Space Agency, 2013). High temporal resolution increases the possibility of frequent image acquisitions during soil freezing and thawing periods, thus overcoming one of the above-mentioned limitations of this study. The recent European Space Agency's (ESA) Soil Moisture and Ocean Salinity (SMOS) mission (Kerr et al., 2010) and the National Aeronautics and Space

Administration's (NASA) Soil Moisture Active and Passive (SMAP) mission (Entekhabi et al, 2010) are dedicated to global soil moisture monitoring using the L-band. The two satellites generate soil moisture products at spatial resolution in kilometres, eg. 43 km for SMOS and 1 km for SMAP. On the other hand, RCM is capable to acquire images at spatial resolution in tens of meters (eg. 50 m) (Canadian Space Agency, 2013) which is more suitable for studies at regional to local scales. All these satellite missions serve to provide information about soil moisture and state depending on different application requirements. With the results presented in this paper, research should continue to further develop understanding of the CP parameters and assist in future use of the CP mode for soil information retrieval.

Chapter 4

Conclusions

This thesis provided a review of QP and CP parameters and conducted a sensitivity analysis of these variables to soil moisture content and freeze/thaw state of an agricultural field in southwest Ontario. A total of 15 RADARSAT-2 images were acquired from October 2013 to June 2014 and CP parameters were synthesized using the acquired RADARSAT-2 QP images. Field measurements were collected along with the radar imagery acquisitions and the continuous *in situ* soil moisture point measurements collected by the Hydra probes were used in the Oh model to simulate radar backscatter. The analysis of the radar backscatter, Oh model estimates and ground measurements gave insights about the microwave interaction at the study site. Results indicated that the C-band radar backscatter in all polarizations can differentiate freeze/thaw state of soils, but their sensitivities to soil moisture content were relatively weak when examining frozen and unfrozen soils separately. The Oh model estimates using the 5 cm ϵ_r measurements matched well with the RADARSAT-2 observations, indicating that the Oh model can be applied for both frozen and unfrozen soils and the study site is similar to bare soils at the C-band. The CP parameters such as S_0, S_3 and $m - \delta$ surface and volume scattering components showed distinct difference between frozen and unfrozen soils. This study demonstrated that the CP mode capable of acquiring images over much larger swaths can potentially be used to large-scale frozen/unfrozen soils mapping.

The novel contribute of this research is the identification of optimal CP parameters for soil moisture and freeze/thaw applications. Improved results can be obtained with more image

acquisitions during the freezing and thawing periods, repetitive image coverage for additional winters, complete measurements of ϵ_r of soils over time and ground measurements collected over wider areas. The existing satellite missions at microwave frequencies, such as SMOS and SMAP, along with the upcoming RCM will acquire more images and offer great opportunities for studying soil moisture and freeze/thaw state at global, regional and local scales. Research should continue to assess the CP parameters and facilitate future use of the CP mode in soil moisture applications. Variables sensitive to soils freeze/thaw state can potentially be used to develop algorithms to classify frozen/unfrozen soils. Thus, future research can focus on evaluating contribution of CP parameters for retrieving soil state information.

References

Adams, J. R., Berg, A. A., McNairn, H., and Merzouki, A. (2013). Sensitivity of C-band SAR polarimetric variables to unvegetated agricultural fields. *Canadian Journal of Remote Sensing,* 39(1), pp. 1–16.

Anderson, D. M. and Tice, A. R. (1971). Low-temperature phases of interfacial water in clay-water systems. *Soil Science Society of America Journal*, 35(1), pp. 47–54.

Baghdadi, N., Gaultier, S., and King, C. (2002). Retrieving surface roughness and soil moisture from synthetic aperture radar (SAR) data using neural networks. *Canadian Journal of Remote Sensing*. 28(5), pp. 701–711.

Baghdadi, N., Nolah, N. and Zribi, M. (2006). Soil moisture estimation using multi-incidence and multi-polarization ASAR data. *International Journal of Remote Sensing*, 27(10), pp. 1907–1920.

Baghdadi, N. and Zribi, M. (2006). Evaluation of radar backscatter models IEM, OH and Dubois using experimental observations. *International Journal of Remote Sensing*, 27(18), pp. 3831–3852.

Baronti, S., Del Frate, F., Ferrazzoli, P., Paloscia, S., Pampaloni, P., and Schiavon, G. (1995). SAR polarimetric features of agricultural areas. *International Journal of Remote Sensing*, 16(14), pp. 2639–2656.

Bernier M. and Fortin J. P. (1998). The potential of times series of C-band SAR data to monitor dry and shallow snow cover. *IEEE Transactions on Geoscience and Remote Sensing*, 36(1), pp. 226–243.

Brubaker, K. L., Entekhabi, D., Eagleson, P. S. (1993). Estimation of continental precipitation recycling. *Journal of Climate*, 6, pp. 1077–1089.

Bruckler, L., Wittono, H. and Stengel, P. (1988). Near surface moisture estimation from microwave measurements. *Remote Sensing of Environment*, 26, pp. 101–121.

Canadian Space Agency. (2011). *Satellite characteristics*. Retrieved from the Canadian Space Agency website http://www.asc-csa.gc.ca/eng/satellites/radarsat/radarsat-tableau.asp.

Canadian Space Agency. (2013). *RADARSAT Constellation*. Retrieved from the Canadian Space Agency website http://www.asc-csa.gc.ca/eng/satellites/radarsat/.

Chamberlain, E. J. and Gow, A. J. (1979). Effect of freezing and thawing on the permeability and structure of soils. *Engineering Geology*, 13, pp. 73–92.

Charbonneau, F. J., Brisco, B., Raney, R. K., McNairn, H., Liu, C., Vachon, P. W., Shang, J., DeAbreu, R., Champagne, C., Merzouki, A., and Geldsetzer, T. (2010). Compact polarimetry overview and applications assessment. *Canadian Journal of Remote Sensing*, 36(2), pp. S298–S315.

Delta-T Devices Ltd. (2007). *User manual for the WET sensor*. Retrieved from the Delta-T Devices Ltd website http://www.delta-t.co.uk/product-downloads.asp?$=Product%20Manuals.

Dingman, S. L. (2002). *Physical Hydrology*, 2nd ed. Upper Saddle River, New Jersey: Prentice Hall.

Dobson, M. C. and Ulaby, F. T. (1986). Active microwave soil moisture research. *IEEE Transactions on Geoscience and Remote Sensing*, 24(1), pp. 23– 36.

Dobson, M. C. and Ulaby, F. T. (1998). Mapping soil moisture distribution with imaging radar. In: F. M. Henderson, & A. J. Lewis (Eds.), *Principles and applications of imaging radar, manual of remote sensing*, 3rd ed, Volume 2, pp. 407–433. New York: Wiley.

Durre, I., Wallace, J. M. and Lettenmaier, D. P. (2000). Dependence of extreme daily maximum temperatures on antecedent soil moisture in the contiguous United States during summer. *Journal of Climate*, 13, pp. 2641–2651.

Entekhabi, D., Njoku, E. G., O'Neill, P. E., Kellogg, K. H., Crow, W. T., Edelstein, W. N., Entin, J. K., Goodman, S. D., Jackson, T. J., Johnson, J., Kimball, J., Piepmeier, J. R., Koster, R. D., Martin, N., McDonald, K. C., Moghaddam, M., Moran, S., Reichle, R., Shi, J. C., Spencer, M. W., Thurman, S. W., Tsang, L., and Van Zyl, J. (2010). The soil moisture active passive (SMAP) mission. *Proceedings of the IEEE,* 98(5), pp. 704−716.

Evans, D. L., Farr, T. G., van Zyl, J. J., and Zebker, H. A. (1988). Radar polarimetry: analysis tools and applications. *IEEE Transactions on Geoscience and Remote Sensing*, 26, pp. 774–789.

Ford, J. P. (1990). Incidence angle and resolution: Potential effects on interpreting Venusian impact craters in Magellan radar images. *Proceedings of the 20th Lunar and Planetary Science Conference*, pp. 573–584.

Geng, H., Gwyn, Q. H. J., Brisco, B., Boivert, J., and Brown, R. J. (1996). Mapping of soil moisture from C-band radar images. *Canadian Journal of Remote Sensing*, 22(1), 117–126.

Gherboudj, I., Magagi, R., Berg, A. A. and Toth, B. (2011). Soil moisture retrieval over agricultural fields from multi-polarized and multi-angular RADARSAT-2 SAR data. *Remote Sensing of Environment*, 115, pp. 33–43.

Hallikainen, M. T., Ullaby, F. T., Dobson, M. C., El-Rayes, M. A., and Wu, L. (1985). Microwave dielectric behavior of wet soil - part 1: Empirical models and experimental observations. *IEEE Transcations on Geoscience and Remote Sensing*, GE-23(1), pp. 25–34.

Hendriks, M. R. (2010). *Introduction to Physical Hydrology*. Oxford, United Kingdom: Oxford University Press.

Hillard, U., Sridhar, V., Lettenmaier, D. P. and McDonald, K. C. (2003). Assessing snow melt dynamics with NASA scatterometer (NSCAT) data and a hydrologic process model. *Remote Sensing of Environment*, 86(1), pp. 52–69.

Hillel, D. (1998). *Environmental Soil Physics*. San Diego, US: Academic Press.

Hoekstra, P. and Delaney, A. (1974). Dielectric properties of soils at UHF and microwave frequencies. *Journal of Geophysical Research*, 79(11), pp. 1699–1708.

Holah, N., Baghdadi, N., Zribi, M., Bruand, A., and King, C. (2005). Potential of ASAR/ENVISAT for the characterization of soil surface parameters over bare agricultural fields. *Remote Sensing of Environment*, 96, pp. 78 − 86.

Jackson, T. J., Kostov, K. G., and Saatchi, S. S. (1992). Rock fraction effects on the interpretation of microwave emission from soils. *IEEE Transactions on Geoscience and Remote Sensing,* 30(3), pp. 610–617.

Jensen, J. R. (2007). *Remote Sensing of the Environment: An Earth Resource Perspective*, 2nd ed. Upper Saddle River, New Jersey: Pearson Prentice Hall.

Jury, W. A. and Horton, R. (2004). *Soil Physics*, 6th ed. Hoboken, New Jersey: John Wiley & Sons.

Kerr, Y. H., Waldteufel, P., Wigneron, J. P., Delwart, S., Cabot, F., Boutin, J., Escorihuela, M. J., Font, J., Reul, N., Gruhier, C., Juglea, S. E., Drinkwater, M. R., Hahne, A., Martin-Neira, M., and Mecklenburg, S. (2010). The SMOS mission: New tool for monitoring key elements of the global water cycle. *Proceedings of the IEEE,* 98(5), pp. 666−687.

Kornelsen, K. C. and Coulibaly, P. (2013). Advances in soil moisture retrieval from synthetic aperture radar and hydrological applications. *Journal of Hydrology*, 476, pp. 460–489.

Li, H., Perrie, W., He, Y., Lehner, S., and Brusch, S. (2013). Target detection on the ocean with the relative phase of compact polarimetry SAR. *IEEE Transactions on Geoscience Remote Sensing*, 51(6), pp. 3299–3305.

McNairn, H., Duguay, C., Brisco, B. and Pultz, T. J. (2002). The effect of soil and crop residue characteristics on polarimetric radar response. *Remote Sensing of Environment*, 80(2), pp. 308–320.

McNairn, H. and Brisco, B. (2004). The application of C-band polarimetric SAR for agriculture: a review. *Canadian Journal of Remote Sensing*, 30(3), pp. 525–542.

Merzouki, A., McNairn, H. and Pacheco, A. (2010). Evaluation of the Dubois, Oh, and IEM radar backscatter models over agricultural fields using C-band RADARSAT-2 SAR image data. *Canadian Journal of Remote Sensing*, 36(2), pp. S274–S286.

Niu, G. Y. and Yang, Z. L. (2006). Effects of frozen soil on snowmelt runoff and soil water storage at a continental scale. *Journal of Hydrometeorology*, 7(5), pp. 937–952.

Nord, M. E., Ainsworth, T. L., Lee, J. S. and Stacy, N. J. S. (2009). Comparison of compact polarimetric synthetic aperture radar modes. *IEEE Transactions on Geoscience Remote Sensing*, 47(1), pp. 174–188.

Oh, Y., Sarabandi, K., and Ulaby, F. T. (1992). An empirical model and an inversion technique for radar scattering from bare soil surfaces. *IEEE Transactions on Geoscience and Remote Sensing*, 30(2), pp. 370–381.

Pivot, F. C. (2012). C-band SAR imagery for snow-cover monitoring at Treeline, Churchill, Manitoba, Canada. *Remote Sensing*, 4(12), pp. 2133–2155.

Presant, E. W. and Wicklund, R. E. (1971). *The soils of Waterloo County*. Research Branch, Canada Department of Agriculture.

Raney, R. K. (1998). Radar fundamentals: technical perspective. In *Principles and applications of imaging radar, manual of remote sensing*. 3rd ed, edited by Henderson, F.M., and Lewis, A.J. John, Volume 2, pp. 9–130. New York: Wiley & Sons, Inc.

Raney, R. K. (2006). Dual-polarized SAR and Stokes parameters. *IEEE Geoscience and Remote Sensing Letters*, 3(3), pp. 317–319.

Raney, R. K. (2007). Hybrid-polarity SAR architecture. *IEEE Transactions on Geoscience Remote Sensing*, 45(11), pp. 3397–3404.

Richards, J. A. (2008). *Radio Wave Propagation: An Introduction for the Non-Specialist*. Berlin: Springer-Verlag.

Richards, J. A. (2009). *Remote Sensing with Imaging Radar*. Heidelberg: Springer.

Schmugge, T. (1985). Remote sensing of soil moisture. In *Hydrological Forecasting*, edited by Baghdadi, M.G. and Burt, T.P., pp.101–124. Chichester: Wiley.

Sellers, P. J., Dickinson, R. E., Randall, D. A., Betts, A. K., Hall, F., Berry, J., Collatz, G., Denning, A., Mooney, H., Nobre, C., Sato, N., Field, C., Henderson-Sellers, A. (1997). Modeling the exchanges of energy, water, and carbon between continents and the atmosphere. *Science*, 275(5299), pp. 502–509.

Seneviratne, S. I., Corti, T., Davin, E. L., Hirschi, M., Jaeger, E. B., Lehner, I., Orlowski, B., and Teuling, A. J. (2010). Investigating soil moisture-climate interactions in a changing climate: a review. *Earth-Science Reviews*, 99(3–4), pp. 125–161.

Shirvany, R., Chabert, M. and Tourneret, J.-Y. (2013). Estimation of the degree of polarization for hybrid/compact and linear dual-pol SAR intensity images: principles and applications. *IEEE Transactions on Geoscience and Remote Sensing*, 51(1), pp.539–551.

Shukla, J. and Mintz, Y. (1982). The influence of land-surface evapotranspiration on the Earth's climate. *Science*, 215 (4539), pp. 1498–1501.

Souyris, J-C., Imbo, P., Fjørtoft, R., Mingot, S., and Lee, J-S. (2005). Compact polarimetry based on symmetry properties of geophysical media: The π/4 mode. *IEEE Transactions on Geoscience Remote Sensing*, 43(3), pp. 634–646.

Stacy, N. and Preiss, M. (2006). Compact polarimetric analysis of X-band SAR data. *Proceedings of 6th European Conference on Synthetic Aperture Radar*. Dresden, Germany: VDE Verlag GMBH.

Stevens Water Monitoring System Inc. (2007). *Comprehensive Stevens Hydra Probe users manual*. Retrieved from the Stevens Water Monitoring System Inc's website http://www.stevenswater.com/catalog/products/soil_sensors/manual/Hydra%20Probe%20Manual%2092915%20June%202007.pdf.

Ulaby, F. T., Baltivala, P. B. and Dobson, M. C. (1978). Microwave backscatter dependence on surface roughness, soil moisture and soil texture: Part 1—Bare soil. *IEEE Transactions on Geoscience and Remote Sensing*, GE-16(4), pp. 286– 295.

Ulaby, F. T., Moore, R. K. and Fung, A. K. (1981). *Microwave Remote Sensing: Active and Passive - Volume 1: Microwave Remote Sensing Fundamentals and Radiometry*. Norwood, MA: Artech House.

Ulaby, F. T., Moore, R. K. and Fung, A. K. (1982). *Microwave Remote Sensing: Active and Passive - Volume 2: Radar Remote Sensing and Surface Scattering and Emission Theory*. Norwood, MA: Artech House.

Ulaby, F. T., Moore, R. K. and Fung, A. K. (1986). *Microwave Remote Sensing: Active and Passive - Volume 3: From Theory to Applications*. Norwood, MA: Artech House.

Ulén, B. (2003). Concentrations and transport of different forms of phosphorus during snowmelt runoff from an illite clay soil. *Hydrological Processes*, 17(4), pp. 747–758.

Willmott, C. J. (1992). Some comments on the evaluation of model performance. *Bulletin American Meteorological Society*, 11, pp. 1309–1313.

Woodhouse, I. H. (2006). *Introduction to Microwave Remote Sensing*. Boca Raton, FL: CRC Press, Taylor & Francis Group.

Zebker, H. A., van Zyl, J. J. and Held, D. N. (1987). Imaging radar polarimetry from wave synthesis. *Journal of Geophysical Research*, 92 (B1), pp. 683–701.